Original Article

Author for correspondence:
Sébastien Wouters,
Email: sebastien.wouters@doct.uliege.be

CAMBRIDGE
UNIVERSITY PRESS

Depositional changes during the Danian–Selandian transition in Loubieng (France), Zumaia (Spain) and Sidi Nasseur (Tunisia): insights from and limits of rock magnetism

Sébastien Wouters[1,2,*] , Simo Spassov[3], Mathieu Martinez[4], Etienne Steurbaut[2,5], Jean-Yves Storme[6], Johan Yans[6] and Xavier Devleeschouwer[2]

[1]Liege University, Sedimentary Petrology, Boulevard du Rectorat, 15, B20, Sart-Tilman, 4000 Liège, Belgium; [2]Royal Belgian Institute of Natural Sciences, O.D. Earth and History of Life, 29 rue Vautier, 1000 Brussels, Belgium; [3]Royal Meteorological Institute of Belgium, Geophysical Centre, rue du Centre Physique, 1, 5670 Dourbes, Belgium; [4]Univ Rennes, CNRS, Géosciences Rennes, UMR 6118, 35000 Rennes, France; [5]KU Leuven, Department of Earth and Environmental Sciences, Celestijnenlaan 200E, 3001 Leuven, Belgium and [6]University of Namur, Department of Geology, Institute of Life, Earth and Environment, ILEE, rue de Bruxelles 61, 5000 Namur, Belgium

Abstract

Depositional changes are studied in three sections encompassing the Danian–Selandian transition, Loubieng (France), Zumaia (Spain) and Sidi Nasseur (Tunisia), using magnetic susceptibility as a proxy. Additional rock-magnetic analyses are used to avoid ambiguous interpretation of magnetic susceptibility. The magnetic susceptibility, measured on 90 to 270 samples per section, is mainly controlled by paramagnetic minerals and linked to detrital input. Major increases in the detrital input are correlated to the end of the Latest Danian Event, a hyperthermal, and to the Danian–Selandian boundary. In Loubieng, two gradual increases in magnetic susceptibility within limestones beds precede the major detrital input increases, and start synchronously with the beginning of the Latest Danian Event and the onset of haematite deposition around the Danian–Selandian boundary, respectively. This haematite is suspected to be of primary origin based, among other things, on low magnetic viscosity values, which is used here as an indicator of diagenetic origin in haematite and goethite. The red levels where haematite is interpreted to be of primary origin could be linked to the hyperthermal event previously hypothesized for the basal Selandian. The comparison of the magnetic susceptibility, chemo- and biostratigraphic data between the three sections highlights the condensed nature of the sedimentation around the Danian–Selandian boundary in the sections of the Atlantic realm. The lower part of the Selandian shows a particularly low sedimentation rate at Zumaia compared to Loubieng and Sidi Nasseur. The latter displays the most complete record of the three.

1. Introduction

The Danian–Selandian transition is a period of climatic change. It witnessed two strong depositional changes that can be linked to climatic processes. The first change, dated at 60.3 Ma, is characterized by the onset of continental deposits in Belgium, the formation of channel systems in Tunisia and non-deposition in Egypt (Steurbaut & Sztrákos, 2008). The second change marks the Danian–Selandian boundary (DSB), which was originally defined as the base of the Lellinge Greensand in Denmark and is now defined as the base of the Itzurun Formation in Zumaia, Spain, its Global Boundary Stratotype Section and Point (GSSP), dated at 59.9 Ma (Steurbaut & Sztrákos, 2008; Schmitz *et al.* 2011). The first depositional change corresponds to the P3a/P3b planktonic foraminiferal subzonal boundary and is correlated to a short-term C isotope negative excursion: the Latest Danian Event, or LDE (Bornemann *et al.* 2009). This event is one of the first of the Palaeogene hyperthermals, i.e. short-term warming events (Bornemann *et al.* 2009; Westerhold *et al.* 2011; Deprez *et al.* 2017). The DSB itself is the beginning of climatic fluctuations, with organic and inorganic stable isotope data suggesting a *c.* 30 kyr hyperthermal event at the very beginning of the Selandian followed by a period of climatic cooling of a few 100 kyr (Storme *et al.* 2014).

In this paper we aim at understanding the depositional changes and the related climatic events occurring around the DSB from coeval sections using rock-magnetic techniques. Rock-magnetic techniques allow the identification, characterization and quantification of magnetic minerals in rocks by measuring magnetic parameters. These parameters can then be used to understand a wide range of geological processes involving these minerals (e.g. Evans & Heller, 2003). For instance, the goethite over goethite plus haematite ratio (G/(G + H)) can be used to determine humidity levels (Abrajevitch *et al.* 2009). Anhysteretic remanent

magnetization (ARM) can be used to quantify low-coercivity minerals like magnetite, titanomagnetite or greigite (Kodama & Hinnov, 2014), whose origin can be interpreted as detrital or biogenic (Moskowitz *et al.* 1993; Kodama *et al.* 2010). Changes in magnetic mineralogy can thus be interpreted as changes in deposition that can in turn be attributed to climatic changes.

The magnetic susceptibility (MS) is one of the most widely used magnetic proxies. Its fast acquisition allows it to be easily used to study the content of magnetic minerals in sedimentary rocks (e.g. Ellwood *et al.* 1999; Mayer & Appel, 1999; Da Silva *et al.* 2013; De Vleeschouwer *et al.* 2015). However, the MS of a sample can be influenced by several types of magnetic minerals that show different behaviours (Kodama & Hinnov, 2014); thus, interpreting a MS signal is not always unequivocal. Typically, both paramagnetic and ferromagnetic minerals (ferromagnetic being used *sensu lato* in this paper) have positive MS values, but for an identical mass the latter have a much higher MS value (Evans & Heller, 2003). Complementary magnetic parameters have to be determined to estimate the contribution to the MS of ferromagnetic, diamagnetic and paramagnetic minerals as well as to provide information about the size, coercivity (i.e. the ability of a ferromagnetic mineral to remain magnetized against an external opposite magnetic field) and type of ferromagnetic minerals. These parameters typically characterize the behaviour of magnetization depending on the magnetic field (e.g. hysteresis loops, isothermal remanent magnetization (IRM)), the temperature or the time.

However, the interpretation of magnetic parameters obtained in weakly magnetic samples such as limestones can be complicated by their high analytical variability. Owing to the low ferromagnetic mineral content in these samples, some of the magnetic parameters will present higher variability than in strongly magnetic materials. Moreover, the magnetic mineralogy may be influenced by a variety of small-scale geological processes that will generate horizontal heterogeneity. This in turn blurs large-scale processes such as the one expected to record climatic variations. This is especially true for parameters influenced by ferromagnetic minerals, as these minerals can form, change and dissolve locally at each step between deposition and cropping out.

The analytical variability of magnetic parameters and the high susceptibility to horizontal heterogeneity make such proxies prone to over-interpretation. Therefore, prior to the depositional changes study, focus will also be set on providing a comprehensive overview of the interpretation of our magnetic parameters, with a focus on the analytical error and on the reproducibility of our results between sections of overlapping age.

Following the work of Storme *et al.* (2014), we study here the same three coeval sections spanning the Danian–Selandian transition: Loubieng (France), Zumaia (Spain) and Sidi Nasseur (Tunisia). The goal is to identify, characterize and compare depositional changes in these sections by using magnetic parameters as proxies. The rock-magnetic data obtained for this study are used together with biostratigraphic and $\delta^{13}C_{org}$ data to provide new constraints on the stratigraphic framework and thus on the changes in the sedimentation rates in the Atlantic and the Tethyan sections around the DSB.

2. Geographical and geological setting

2.a. The Zumaia GSSP section

The Zumaia sea-cliff section contains the GSSP for the base of the Selandian Stage (also referred to as the DSB; Schmitz *et al.* 2011).

It is located on Itzurun beach, *c.* 500 m to the northwest of Zumaia city centre, in Spain (43° 18' 5" N, 2° 15' 35" W; Fig. 1b; Storme *et al.* 2014). A long sequence of rocks of Late Cretaceous to early Palaeogene age crop out along the beach, the Palaeocene being represented by 165 m thick hemipelagic deposits (Schmitz *et al.* 2011). The palaeogeographical position of the section is in the Bay of Biscay, in the Atlantic realm (Fig. 1d). The section spans the upper part of the Danian Aitzgorri Limestone Formation and the lower part of the Selandian Itzurun Formation (Schmitz *et al.* 2011). An important lithological change occurs at the boundary between the two formations where the reddish marl of the Selandian overlies the greyish-to-reddish alternating marl and limestone beds of the Danian. This lithological change defines the base of the Selandian (Schmitz *et al.* 2011), and coincides with bio-event E4 (Storme *et al.* 2014), i.e. the end of the acme of *Braarudosphaera* and the lowest consistent occurrence of *Lithoptychius* aff. *bitectus* (*Fasciculithus janii sensu* Steurbaut & Sztrákos, 2008). The hemipelagic sediments were deposited at an estimated water depth of between 900 and 1100 m (Arenillas *et al.* 2008). A total of 89 samples were studied here. Some of the C and O stable isotope measurements were already presented in Storme *et al.* (2014) (Table 1). The sampling interval is irregular, ranging from 0.10 to 2.75 m.

2.b. The Loubieng section

The Loubieng section is located in the North Pyrenean Tectonic Zone westward of Pau, in France (Henry *et al.* 1989; Storme *et al.* 2014). It is an abandoned quarry located 300 m to the east of the junction between route départementale D947 Orthez–Navarrenx and route départementale D110 Loubieng–Sauvelade (43° 25' 38" N, 0° 44' 37" W; Fig. 1a). It is formed by several faulted blocks marked by small displacements along normal faults. It was investigated in the past for biostratigraphy (Peybernès *et al.* 2000; Steurbaut & Sztrákos, 2008; Storme *et al.* 2014), stable isotopes (Storme *et al.* 2014) and cyclostratigraphy (Dinarès-Turell *et al.* 2010). Palaeomagnetic measurements were carried out; however, the primary remanent magnetization record was overprinted by a consistently reverse component of unknown age blocked in low-coercivity minerals (Dinarès-Turell *et al.* 2010). The lower part of the section belongs to the upper part of the Lasseube Formation (Steurbaut & Sztrákos, 2008; Storme *et al.* 2014). It forms the quarry front and consists of an alternation of almost horizontally bedded limestone beds and marl intercalations. As in Zumaia, the lithology evolves from carbonates to fine-grained siliciclastic deposits from the Danian towards the Selandian. This is most obvious at the boundary between the limestone beds of the Lasseube Formation and the overlying marl and clays of the Pont-Labau Formation (Latapy Member). The DSB has been placed at this formation boundary by Steurbaut & Sztrákos (2008). It also coincides with bio-event E4 (Storme *et al.* 2014). The palaeogeographical position of the Loubieng deposits is in the Bay of Biscay, in the Atlantic realm (Fig. 1d; Storme *et al.* 2014). The depositional depth of the sediments has been estimated to be more than 600 m (Steurbaut & Sztrákos, 2008). A bed-to-bed correlation of the Danian interval between the Loubieng, Zumaia and Bjala (Bulgaria) sections was established by Dinarès-Turell *et al.* (2010) on the basis of lithologic stacking patterns that represent eccentricity orbital cycles, with limestone–marl couplets representing precession cycles.

The first batch of samples (namely, B1) was initially collected in marl and claystone beds by Steurbaut & Sztrákos (2008). Batch B1

Table 1. Details of C and O isotope analyses

Section	Samples	Measurement	Height	Publication
Zumaia	08ZM, 10ZM, 11ZM	2012–2013	−20 to −2.5 m	This paper
			−2.5 to 22 m	Storme *et al.* (2014)
Loubieng	LOU	2015 (B2)	3 to 12 m	This paper
	LO	2012–2013 (B1)	0 to 13 m	This paper
			13 to 32 m	Storme *et al.* (2014)
Sidi Nasseur	NSF, NSC, 08NSI, 10NSC	2012–2013	0 to 21 m	This paper
			21 to 68 m	Storme *et al.* (2014)
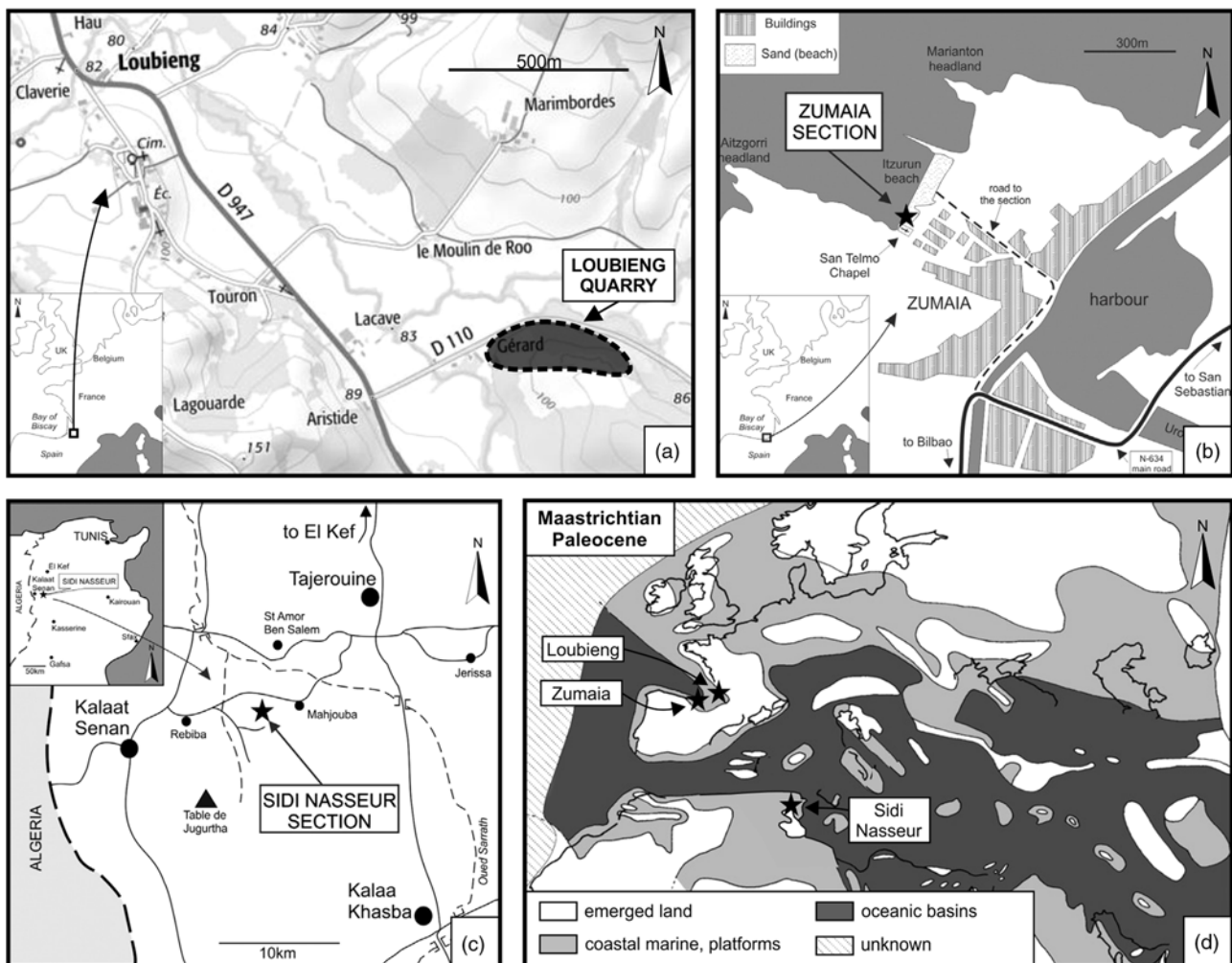
Fig. 1. Location of the (a) Loubieng (Bureau de Recherches Géologiques et Minières maps database, available at http://infoterre.brgm.fr/viewer/MainTileForward.do; accessed 11 February 2015), (b) Zumaia and (c) Sidi Nasseur sections (Storme *et al.* 2014). (d) Palaeogeographical context during Maastrichtian and Paleocene times (modified from Gheerbrant & Rage, 2006 following Storme *et al.* 2014).

was used for C and O isotope geochemistry and biostratigraphy analyses. Parts of these results were presented in Storme *et al.* (2014), and are reworked in this study as part of a larger set of measurements on batch B1 (Table 1). Additionally, we collected samples every 0.10 m through the Danian and basal Selandian, and every 0.25 m in the upper part of the Selandian to provide a second batch of samples (batch B2; Table 1) representative of all lithologies present in the section. Batch B2 contains 266 samples, making Loubieng the most completely sampled section of

the three. However, the sampling resolution is not sufficient to allow the robust detection of short-term cycles (Martinez *et al.* 2016), which is beyond the scope of this study.

2.c. The Sidi Nasseur section

The Sidi Nasseur section is located between Kalaat Senan, Tajerouine and Kalaa Khasba in Tunisia, close to the Algerian border (35° 48' 18" N, 8° 26' 48" E; Fig. 1c; Storme *et al.* 2014). It is a

composite section, formed by four subsections (namely, NSC, 10NSC, NSF and 08NSI), exposed on the flank of an incised gully (Storme et al. 2014). The sediments are marl-shales deposited in a neritic environment and form part of the El Haria Formation (Guasti et al. 2006; Van Itterbeeck et al. 2007). Intercalations of limestone and indurated marl can also be found (Storme et al. 2014). Palaeogeographically it belongs to the southern Tethys realm, near Kasserine island, which supplied significant terrigenous input (Fig. 1d; Guasti et al. 2006). The position of the DSB in the section was proposed at 38.5 m by Storme et al. (2014) based on the bio-event E4. A total of 149 samples were studied here. Some of them provided C and O stable isotope measurements that were presented in Storme et al. (2014) (Table 1). The sampling interval is irregular in the lower part of the section (in the NSC, 10NSC and NSF subsections), with a range of from 0.20 to 1.75 m between samples, but the upper part was sampled regularly every 0.25 m (in the 08NSI subsection).

3. Materials and analytical methods

3.a. Biostratigraphy

The foraminiferal and calcareous nannofossil biostratigraphic interpretations of the Zumaia, Sidi Nasseur and Loubieng sections are based on bio-events E1 to E7 as defined by Storme et al. (2014), essentially relying on Schmitz et al. (2011) for the Zumaia section and on Steurbaut & Sztrákos (2008) for the Loubieng section. Additional calcareous nannofossil investigations were carried out on six samples from the Loubieng section to pinpoint the second radiation of the fasciculiths (FR2; Schmitz et al. 2011), which was not discussed previously for this section, and to verify the position of E5. Four additional samples were collected in the uppermost 2 m of the Danian (25b, 27a, 27c and 27d at 17.73, 18.41, 18.85 and 19.20 m, respectively) and two in the lowermost 9 m of the Selandian (29b at 26.87 m and 32a at 31.5 m). The biozonation and taxonomy adopted here were detailed in Storme et al. (2014). Smear slides and samples are stored in the collections of the Royal Belgian Institute of Natural Sciences (Brussels, Belgium).

3.b. Sample colour determination

Standard lithological and colour observations were made to use as a reference against the magnetic parameters. Sample colour determination was achieved by visual comparison of humidified samples with a Munsell chart adapted for geological purposes (Goddard et al. 1948). Colours are classified by a code, giving the hue, lightness and chroma, and by a name from the ISCC-NBS classification (in italics in this article). Some sample sections were polished to observe the distribution of colour using optical microscopy.

3.c. Instrumentation for magnetic measurements

Low-field magnetic susceptibility (X_{LF}) was measured with a Kappabridge MFK1-A (AGICO) installed at the Royal Belgian Institute of Natural Sciences (RBINS) and set at a field intensity of 400 A m^{-1} and a frequency of 976 Hz. The sample mass for these measurements (c. 10 g) was determined with a 1 mg precision weighing scale. Induced and remanent isothermal magnetization curves were measured with an induction coercivity meter (J-meter; Evans & Heller, 2003) at the Royal Meteorological Institute of Belgium (RMIB). The J-meter works in a range of magnetic fields limited to ± 500 mT. Additional magnetic techniques were further

performed at much higher magnetic fields to study the influence of high-coercivity minerals on X_{LF} and on the J-meter measurements. The additional analyses were performed using a Magnetic Property Measurement System MPMS 3 (Quantum Design), which is installed at the RMIB and can reach magnetic fields of up to 7 T. In each of the sections, 40 to 55 samples were selected and measured with the J-meter. From those samples measured using the J-meter, 13 were further selected to be studied using the MPMS 3 (four from Zumaia, nine from Loubieng). For these types of measurements, the sample mass was determined using a laboratory weighing scale with a precision of 0.02 mg. Typical sample masses were in the order of 1 g and 25 mg, for the J-meter and the MPMS 3 measurements, respectively. The J-meter measurement sequence is explained in detail in Devleeschouwer et al. (2010).

3.d. Magnetic parameters calculation

3.d.1. Parameters related to magnetic susceptibility

The high-field magnetic susceptibility (X_{HF}) estimates the contribution of diamagnetic and paramagnetic minerals to X_{LF}. X_{HF} is obtained from a linear regression on the induced magnetization curve at high magnetic fields (Equation 1). In this study, the high-field interval ranges from c. 0.3 to c. 0.5 T (the precise interval is adjusted for each sample to avoid artefacts in case of low signal-to-noise (S/N) ratio).

$$X_{HF} = \frac{dM_i(H)}{\mu_0 \, dH} \qquad (1)$$

where M_i is the induced magnetization intensity, H the magnetizing field and μ_0 is the magnetic permeability of a vacuum. With the magnetic fields of less than 0.5 T reached by the J-meter, the presence of high-coercivity minerals such as haematite, goethite or pyrrhotite (Dekkers, 2007) can also increase the value of X_{HF}. The X_{ferri} parameter quantifies the contribution to X_{LF} of ferrimagnetic (or low-coercivity) minerals such as magnetite, maghaemite and greigite. X_{ferri} is obtained by subtracting X_{HF} (estimating the contribution of diamagnetic, paramagnetic and high-coercivity minerals) from X_{LF}, as the ferrimagnetic minerals are considered saturated in a field above 0.3 T (Dekkers, 2007).

3.d.2. Parameters for viscous remanence decay

The viscous remanence decay is the decrease of remanent magnetization with time. It is measured during the final measurement step of the J-meter sequence and is related to the occurrence of magnetically viscous grains, depending on their size. Viscous behaviour can be observed in multidomain (MD) grains, large enough to have several magnetic domains. Magnetic minerals around the superparamagnetic (SP)/stable single domain (SSD) grain-size boundary (c. 20–30 nm at 25 °C) also display viscous behaviour (Néel, 1949; Liu et al. 2005). In these SP/SSD grains, the viscous effect is usually much more pronounced than in MD grains. Magnetic minerals below the SP/SSD grain-size boundary are superparamagnetic and lose their remanent magnetization before it can reliably be observed with our instruments. Conversely, SSD grains do not show such an effect within typical observation times, i.e. seconds to weeks. This is due to magnetization decay of a magnetic grain following an exponential law in relation to grain size. The overall viscous decay of a sample is quantified by the dimensionless parameter S_d (Dunlop, 1973; Wang et al. 2010):

$$S_d = \frac{dM_{r\ relative}(log(t))}{dlog(t)} \quad (2)$$

where $M_{r\ relative}$ is the remanent magnetization intensity normalized to its initial value at 0 s. In the case of the J-meter measurements, the magnetization values were normalized to M(t = 0.4 s), because the magnet needs 0.4 s to drive the field down from 500 to 0 mT. The S_d parameter was calculated here with a similar time interval for all samples, from 0.4 to 100 s.

3.d.3. Parameters related to the saturation of ferromagnetic minerals

The J-meter device can reach fields of up to 0.5 T, which exceed the saturation magnetic field of most of the low-coercivity minerals. This magnetic field is nonetheless not strong enough to saturate the high-coercivity minerals. We define here the ΔIRM and the high-coercivity mineral contribution (HCMC) parameters to estimate their contribution to the IRM at the maximum field available (Devleeschouwer *et al.* 2015):

$$\Delta IRM = IRM_{-0.5T} - IRM_{-0.3T} \quad (3)$$

$$HCMC(\%) = 100\% * \frac{\Delta IRM}{IRM_{-0.5T}} \quad (4)$$

ΔIRM is not normalized, and should be used compared to the IRM at 0.3 T and/or 0.5 T. Note that high-coercivity minerals can display magnetization over the whole field spectrum and thus contribute to the $IRM_{-0.3\ T}$ value (Equation 3). In addition, the maximum available field is limited to 0.5 T; contributions of high-coercivity minerals at higher fields are thus not detected. For these reasons, high values in HCMC and ΔIRM underestimate the actual proportion of high-coercivity minerals and must be considered rather as an approximation of the contribution of high-coercivity minerals to the total remanence of the sample. In this study, HCMC and ΔIRM are calculated from the backfield curve, which justifies the negative magnetic field values used in Equations 3 and 4. This approach allows all samples to go through a similar initial magnetization at 0.5 T and minimizes the effect of any natural remanent magnetization left in the sample at −0.5 T.

3.d.4. Hysteresis parameters

Four parameters usually characterize hysteresis loops: saturation remanent magnetization (M_{rs}), coercivity of remanence (H_{cr}), saturation magnetization (M_s) and coercive force (H_c). M_{rs} and H_{cr} can be obtained from the remanent magnetization data and are not influenced by dia- and/or paramagnetic contributions. M_{rs} is equivalent to the $IRM_{-0.5\ T}$ if saturation is attained at −0.5 T, and H_{cr} is obtained by finding the field value at zero remanent magnetization. Usually, M_{rs} is determined from the hysteresis loop (i.e. from induced magnetization data), but in this study it was calculated from the remanent magnetization at the maximum field of 0.5 T if saturation is reached. This is a more accurate determination because the hysteresis measurement is influenced by the remanent field of the electromagnet. Conversely, remanent magnetization is measured in a magnetically shielded induction coil outside of the electromagnet.

Natural samples often contain significant amounts of dia- and/or paramagnetic minerals, both having a linear induced magnetization dependence to the magnetic field. A high-field slope correction can be applied to induced magnetization data to subtract the contribution of dia- and/or paramagnetic minerals, following Equation 5:

$$M_{i\ corrected}(H) = M_i(H) - \mu_0 * H * X_{HF} \quad (5)$$

where $M_{i\ corrected}$ is the corrected induced magnetization. From $M_{i\ corrected}$, M_s can then be determined as the $M_{i\ corrected}$ at 0.5 T, and H_c as the field value where $M_{i\ corrected}$ is zero. This correction only applies when the saturation is reached between 0.3 and 0.5 T. Otherwise, high-coercivity minerals would also contribute to X_{HF} and mislead the correction. If the HCMC exceeds the arbitrarily chosen threshold of 5 %, we consider that saturation is not reached. In that case, the parameters M_{rs}, $M_{i\ corrected}$, M_s and H_c are incorrect and not taken into account.

3.d.5. Variability and uncertainty calculation

The calculations of the several magnetic parameters used in this study rely on isothermal magnetization curves that are measured with a J-meter. Because of the low magnetic content of the samples, the obtained magnetization curves are relatively noisy, especially for the induced magnetization at high fields. At a field of *c.* 0.4 T, the S/N ratio is typically about 0.75 for samples with an induced magnetization of 2 to 4 mA m² kg⁻¹ (typically the limestone samples in this study). The weakest samples have a S/N ratio of *c.* 0.50. The data is thus smoothed, applying a linear regression on specific magnetic field intervals (e.g. around 0 mT for M_{rs}, around H_{cr}, etc.). The magnetic field intervals chosen for smoothing are adapted on a visual basis for each sample to compensate for noise without creating artefacts. The variability of the parameters is different for each sample and is especially high in weakly magnetic samples such as the limestones studied here. To account for this, measurements and parameter calculations were done three times and averaged. The standard deviation of the three samples was calculated using the central limit theorem, allowing the variability of the parameters to be estimated for each sample separately.

3.d.6. High-field (7T) hysteresis

Some samples from the Loubieng and Zumaia sections showed evidence of the presence of high-coercivity minerals. High-field hysteresis loops (up to 7 T) were performed on 13 of these samples to study their saturation at high fields using the remanent hysteretic magnetization (M_{rh}; Fabian & von Dobeneck, 1997):

$$M_{rh}(H) = \frac{M^+(H) - M^-(H)}{2} \quad (6)$$

where M⁺ and M⁻ are the upper and lower branches of the hysteresis. M_{rh} accounts for the opening of the hysteresis curve and its calculation does not require slope correction (e.g. Fig. 2g–i). If the sample is saturated, the hysteresis loop should be closed and M_{rh} should stabilize to zero in the high-field ranges.

3.d.7. Temperature dependence of remanent magnetization

The same 13 samples were analysed for their temperature dependence of remanent magnetization (e.g. Fig. 2a–f). Before measurement, the samples were magnetized at 'room temperature' (27 °C or 300 K) in a 7 T field. Then the field was switched off and a waiting time of 10 min was applied to minimize the viscous remanent magnetization contributions to the total remanent magnetization. After that, the remanent magnetization was measured during a low-temperature cycle from 27 °C to −173 °C (300 to 100 K) and back to 27 °C. A second measurement was carried out, during a high-temperature cycle from
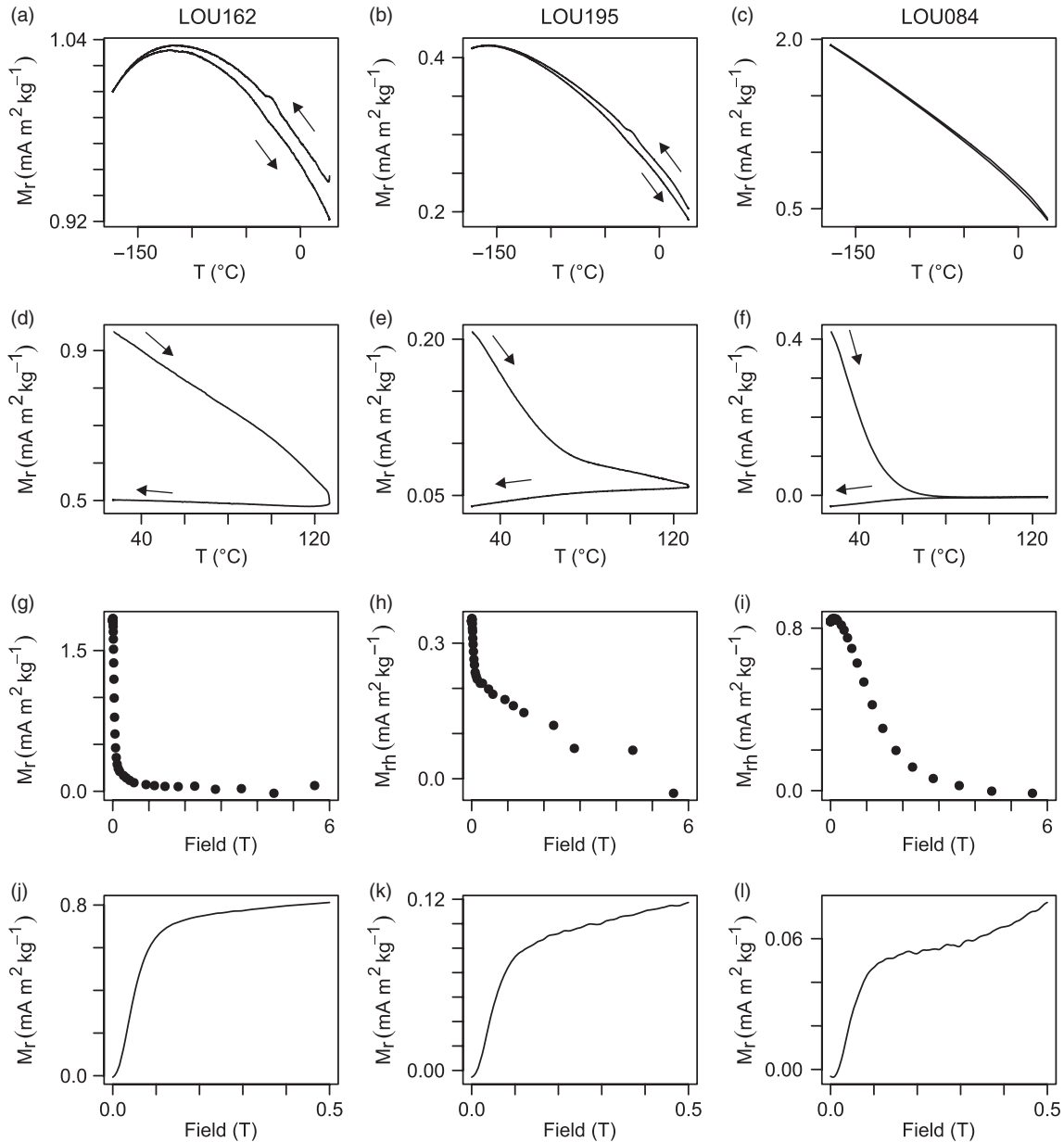
Fig. 2. Comparison of magnetic analyses of selected samples from Loubieng section, where high-coercivity minerals are present: in sample LOU162 haematite, in sample LOU195 a mixture between haematite and goethite and in sample LOU084 goethite. (a–f) Remanent magnetization versus temperature (measured with the MPMS 3). The small fluctuation observed at −25 °C is interpreted as the Morin transition that is characteristic for haematite. Goethite-bearing samples have a more linear and reversible cooling cycle, and goethite loses its remanence before 80 °C during the warming cycle. (g–i) M_{rh} of a hysteresis at 7 T (measured with the MPMS 3). Only half of the hysteresis is represented. Goethite samples do not saturate, but in the goethite-dominated sample (LOU084) remanence decreases smoothly well before 6 T. (j–l) IRM of the samples (measured with the J-meter), with a higher coercivity component in LOU084 relative to the other samples (goethite). The partial saturation at 0.3 T also indicates the presence of low-coercivity minerals in all three samples.

27 °C to 127 °C (400 K) and back to 27 °C. The sample was prepared before the second measurement with another 7 T remanence acquisition at 27 °C followed by a 10 min waiting time.

From the latter analysis, the goethite contribution (GC) to the remanent magnetization was calculated. It relies on goethite having an unblocking temperature (T_b) of lower than 110 °C, and on the assumption that the remanence after T_b can be used to approximate the remanence behaviour of haematite and of low-coercivity minerals before T_b (see also Dekkers, 1989). The unblocking temperature is here used rather than the Néel temperature (120 °C; Özdemir & Dunlop, 1996), as the latter is too close to the maximum temperature reached by the MPMS 3 (400 K or 127 °C). The

remanence between T_b and the maximal temperature that the MPMS 3 reaches (i.e. 127 °C) is modelled by a linear function for which the parameters *a* and *b* are determined by linear regression:

$$M_r^{model}(T) = aT + b \tag{7}$$

Next, this function was extrapolated to 27 °C and the GC parameter was calculated as follows:

$$GC = 100\% * \frac{M_r^{total}(27°C) - M_r^{model}(27°C)}{M_r^{total}(27°C)} \tag{8}$$
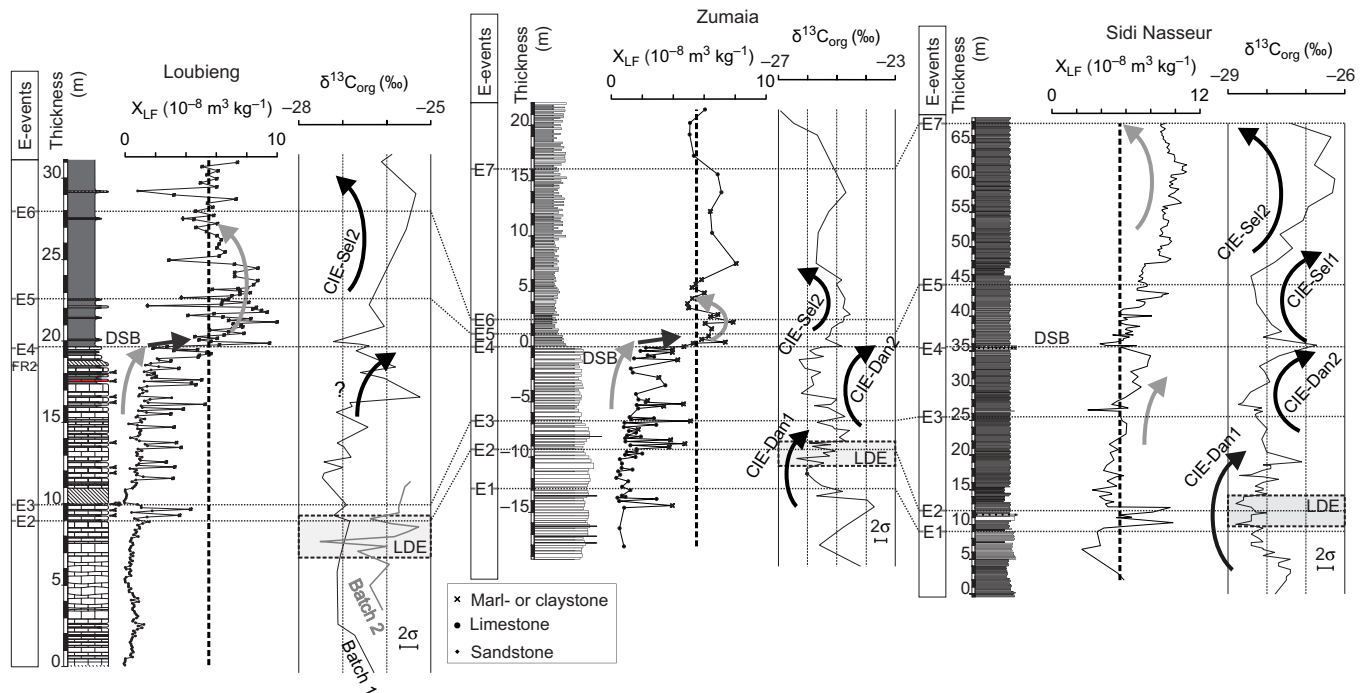
Fig. 3. Comparison between magnetic susceptibility, organic carbon isotopes (δ¹³C_org) and biostratigraphic E-event results for the Loubieng, Zumaia and Sidi Nasseur sections (partly based on Storme *et al.* 2014). DSB – Danian–Selandian boundary; LDE – Latest Danian Event; FR2 – second radiation of fasciculiths; E – bio-events.

3.e. Organic carbon isotope (δ¹³C_org) measurements

The methodology to measure the δ¹³C_org is the same as in Storme *et al.* (2014): samples were powdered, acidified in 25 % HCl for 2 hours to remove carbonates and centrifuged repeatedly with deionized water until a neutral sediment was obtained. The remainder was dried and powdered again. These treated samples were then weighed in tin capsules, which were rolled into balls and measured for δ¹³C_org using a Carlo Erba EA1110 elemental analyser coupled to a Thermo Finnigan Delta plus XP mass spectrometer. Carbonates and total organic carbon contents were measured with a Bernard calcimeter and a standard LECO carbon analyser (CS-200), respectively. The variability of repeated δ¹³C_org measurements was 0.4 ‰ (2σ) on laboratory standards and selected samples.

Two batches of samples were processed and measured separately for organic carbon isotope (δ¹³C_org) measurements; see Table 1 for further details. As they were measured separately, there might be a slight offset of δ¹³C_org absolute values between these two batches owing to calibration differences.

4. Results

4.a. Biostratigraphy

4.a.1. Loubieng

The calcareous nannofossil investigation of the six additional samples from the Loubieng section (Fig. 3) confirms the biostratigraphic interpretation of Storme *et al.* (2014). The following bio-events are identified (Fig. 3):

- *Bio-event E2 at 8.95 m.* This event coincides with the calcareous nannofossil subzonal NTp7a and NTp7b boundary defined by Varol (1989). It corresponds to the first radiation of *Fasciculithus* (Bernaola *et al.* 2009).
- *Bio-event E3 at 9.80 m.* It corresponds to the NTp7b and NTp8a boundary (Varol, 1989).

- *Bio-event E4 at 19.70 m.* It corresponds to the end of the acme of *Braarudosphaera* and marks the DSB.
- *Bio-event E5 at 22.60 m.* It is defined by the lowest occurrence of *Fasciculithus tympaniformis*.
- *Bio-event E6 at 27.95 m.* It corresponds to a major decrease in *Morozovella*.

The present study also pinpoints the second influx of various *Lithoptychius* species, known as the second *Fasciculithus* radiation (Bernaola *et al.* 2009; Schmitz *et al.* 2011) at exactly 18.70 m, between samples 27a (new) and 27b (former sample 27 of Steurbaut & Sztrákos, 2008), respectively.

It should be noted that the position of E2 lacks precision owing to the scarcity of suitable material (clay or marl) in this interval and could be located in the 2 m below. Its position is justified here as it is coherent with what is observed in the Zumaia section.
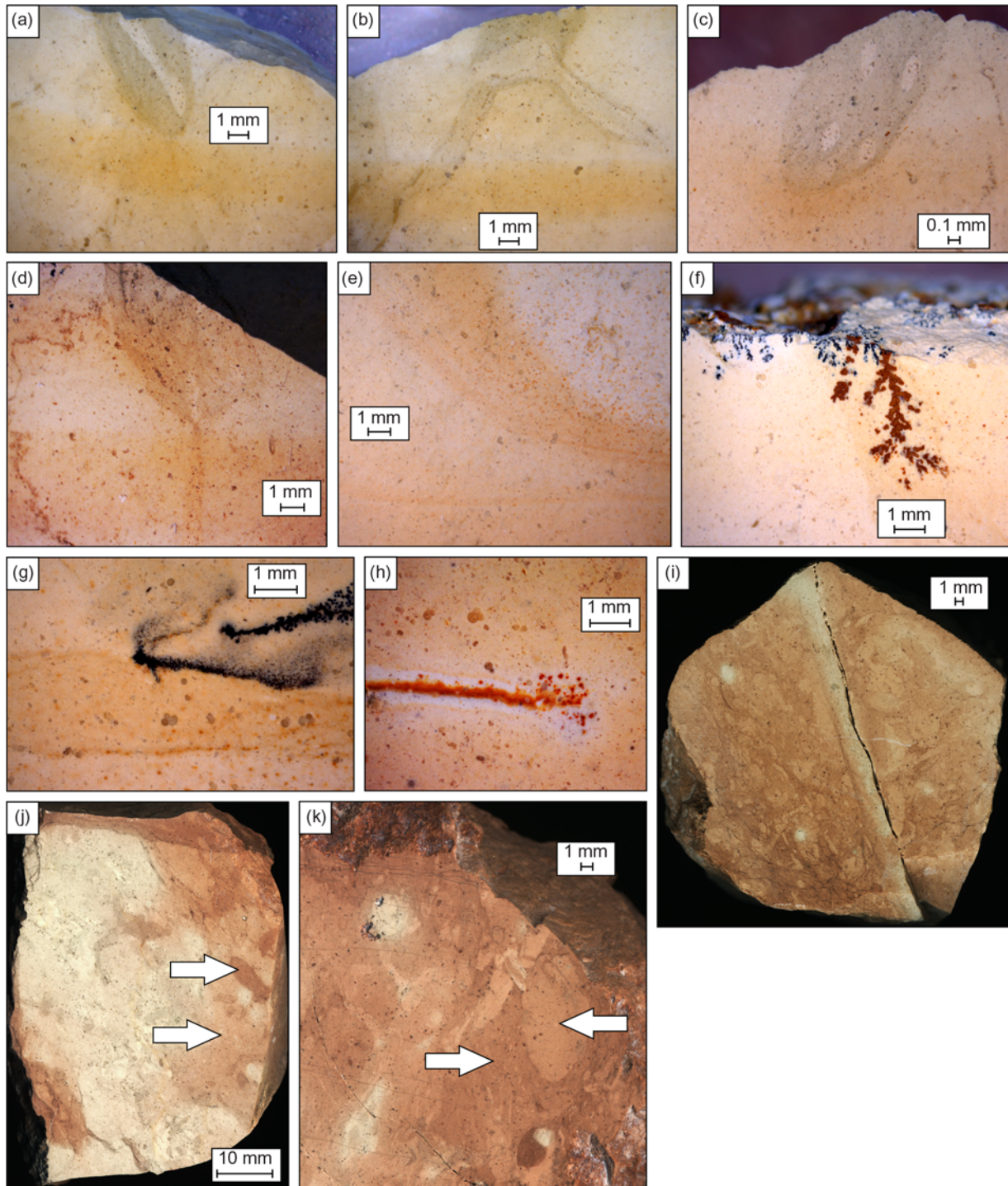
4.b. Colour

4.b.1. Loubieng

At Loubieng, the sediment colour mostly depends on the lithology. Limestone beds are *white* (N9), *very light grey* (N8) or in the majority *yellowish grey* (5Y 8/1). Marl and claystone ranges from *yellowish grey* (5Y 8/1) to *olive grey* (5Y 4/1). However, 54 'yellow' samples and 11 'red' ones break this strict link to lithology: they are encountered as coloured levels whose stratigraphic extent is independent from the limestone and marl beds. Note that the denomination of levels as 'yellow' and 'red' used generally in this study is based on their hue and their magnetic mineralogy (see Section 4.e) and is not part of the ISCC-NBS classification.

The 'yellow' samples have a hue of 10YR in the Munsell system and range from 10YR 8/2 (*very pale orange*) to 10YR 8/5 (10YR 8/6 being *dark yellowish orange*). 'Yellow' samples have a particularly strong chroma (up to 6 in the chromatic scale) between 7 and 9 m. The 'yellow' colour is observed in polished sections as milli- to

Fig. 4. (Colour online) (a–d) 'Yellow' levels overprinting bioturbation. (e) Non-parallel 'yellow' levels. (f–h) Oxide remineralizations and discolouration around these reminer-alizations (h). (i–k) 'Red' samples with strong mixing due to bioturbation, highlighted by several shades of 'red' (arrows). Discolouration is also observed in these samples close to a fracture (i).

centimetre-wide bands that are not necessarily parallel (Fig. 4e), overprinting bioturbation (Fig. 4a–d). The colour is sometimes more pronounced near bioturbation (Fig. 4a, c, d). Oxides can be found disseminated in the bulk rock: orange iron oxides and black manganese oxides (Fig. 4f–h). The rock can sometimes be discoloured (Fig. 4h). The 'red' samples have a hue of 10R or 5YR. Colours are *pale red* (10R 6/2) in limestone and range from *moderate brown* (5YR 4/4) to *light brown* (5YR 6/4) in marl and

claystone. These 'red' levels are found between 16 and 20 m. Bioturbation strongly mixes different shades of 'red' (arrows in Fig. 4j, k), and near small fractures discolouration can be seen (Fig. 4i).

4.b.2. Zumaia

At Zumaia 'grey' and 'red' samples can be identified. 'Grey' samples display colours from *medium grey* (N5) to *yellowish grey* (5Y 8/1).

Twenty-three 'red' samples have a hue of 5R, 10R or 5YR and colours between *greyish red* (10R 4/2) and *pale red* (10R 6/2), or between *pale brown* (5YR 5/2) and *pinkish grey* (5YR 8/1). Two 'yellow' samples were found, with a hue of 10YR. As in Loubieng, bioturbation is highlighted by colour contrasts.

4.b.3. Sidi Nasseur
The Sidi Nasseur section samples are very monotonous in lithology and colour. They are therefore not characterized by colour any further.

4.c. Magnetic susceptibility

4.c.1. Loubieng
The Loubieng section can be divided into the three following intervals based on lithology and X_{LF} (Fig. 5):

(1) The first interval is dominated by limestone beds from the bottom of the section up to 8.95 m at E2. X_{LF} values are generally under 1×10^{-8} m^3 kg^{-1}. Ferrimagnetic minerals contribute significantly but monotonously to X_{LF}, as the X_{ferri} values can reach up to 0.6×10^{-8} m^3 kg^{-1} and remain broadly constant. X_{HF} values, representing paramagnetic minerals, vary between *c.* 1×10^{-10} m^3 kg^{-1} and 0.6×10^{-8} m^3 kg^{-1}. The amplitudes of variations of X_{HF} are much higher than the variations of X_{ferri}; thus, fluctuations in X_{HF} are at the source of the changes in X_{LF}. X_{HF} values gradually reach two local maxima: (i) at 2.5 m, where two marlstone beds intercalate within the limestone beds, and (ii) at 8.95 m, where the onset of marl–limestone alternations mark stronger detrital input (Fig. 5). All these values remain low, implying low contents of paramagnetic and ferromagnetic minerals in this interval.

(2) The second interval is characterized by marl–limestone alternations observed from E2 at 8.95 m to the DSB at 19.70 m. The X_{LF} values generally exceed 3×10^{-8} m^3 kg^{-1} in marl beds, while they rarely exceed 2×10^{-8} m^3 kg^{-1} in the limestone beds. However, at the top of this second interval, two 'red' limestone samples at 16.5 and 19 m have X_{LF} values higher than 3×10^{-8} m^3 kg^{-1} and 2×10^{-8} m^3 kg^{-1}, respectively, while two marl samples at *c.* 18 m have X_{LF} values close to 2×10^{-8} m^3 kg^{-1}. In the two 'red' limestone samples, high X_{ferri} values are observed, indicating the presence of ferrimagnetic minerals as the source of the high X_{LF} values. From 15 m to the DSB, the X_{LF} values in the limestone beds generally increase, reflecting the increasing dominance of the detrital input in the sedimentation.

(3) Prevalent marl and claystone characterizes the third interval. Above the DSB, X_{LF} values generally exceed 4×10^{-8} m^3 kg^{-1}, and reach up to 8×10^{-8} m^3 kg^{-1} in the interval between the DSB and 25 m. Above 25 m, the X_{LF} values decrease and stabilize at *c.* 6×10^{-8} m^3 kg^{-1}.

Beyond these broad trends, distinct beds show particularly low X_{LF} values. These beds are:

(1) Massive limestone beds having X_{LF} values ranging from -0.1 to 0.1×10^{-8} m^3 kg^{-1} and marked by particularly low values at their bottoms. Two of these limestone beds are found from 0 to 0.6 m and from 10 to 11 m (B1 and B2; Figs 5, 6). Additionally, limestone beds are found with X_{LF} values lower than 0.1×10^{-8} m^3 kg^{-1} from 4 to 7 m, within an interval where lenticular bedding is observed.

(2) Sandstone and limestone beds in the Selandian part of the section with X_{LF} values below or *c.* 4×10^{-8} m^3 kg^{-1}. They crop out in the field as more indurated beds within the softer marl and claystone dominating in that interval.

4.c.2. Zumaia
Based on lithology and X_{LF}, the Zumaia section can be divided into three intervals (Fig. 7):

(1) A limestone-dominated interval from the bottom of the section (-18 m) to -10 m, which mainly displays low X_{LF} values of *c.* 1×10^{-8} m^3 kg^{-1}. Thin marl layers were observed, but the large sampling interval did not allow their detailed study.

(2) An interval of marl–limestone alternations, from -10 m up to the DSB at 0 m. Marl samples generally have higher X_{LF} values (more than 2×10^{-8} m^3 kg^{-1}) than the limestone ones (X_{LF} values *c.* 2×10^{-8} m^3 kg^{-1}). Two marl samples have, however, lower X_{LF} values than the average limestone at -7.5 and -5 m, and three limestone samples have higher X_{LF} than the average marl at -7, -6.5 and -3.5 m. From -12 m (in the first interval) to the DSB, the limestone X_{LF} values tend to increase progressively from 1.5×10^{-8} m^3 kg^{-1} to 2×10^{-8} m^3 kg^{-1}, indicating an upward increase in the detrital fraction in the sediment.

(3) Above the DSB, X_{LF} values suddenly increase to *c.* 6×10^{-8} m^3 kg^{-1} in an interval with a more important terrigenous component. These values are far above the values observed in the Danian. A maximum value of *c.* 8×10^{-8} m^3 kg^{-1} is reached right above the DSB. The X_{LF} values then decrease to 5×10^{-8} m^3 kg^{-1} at 4 m, and increase again to 8×10^{-8} m^3 kg^{-1} at 8 m. After these rapid fluctuations, the X_{LF} values gently decrease to 6×10^{-8} m^3 kg^{-1} at the top of the section.

Generally, X_{HF} is higher than X_{ferri}, so that X_{LF} mainly reflects a paramagnetic signal. However, 12 'red' samples are characterized by X_{ferri} values higher than their X_{HF}. The high X_{ferri} values in these samples indicate the presence of ferrimagnetic minerals, and raises the X_{LF} above the values expected for the respective lithologies.

4.c.3. Sidi Nasseur
The Sidi Nasseur section displays a smooth, long-term trend in increasing X_{LF} values from the bottom of the section (X_{LF} *c.* 5×10^{-8} m^3 kg^{-1}) to the DSB, overlain by minor fluctuations (Fig. 8). Through the DSB the values locally decrease with an amplitude of 4×10^{-8} m^3 kg^{-1} and then continue to increase. This increase in X_{LF} values reaches a maximum of 11×10^{-8} m^3 kg^{-1} at 62 m, followed by a smooth decrease of X_{LF} values until the end of the section (down to 9×10^{-8} m^3 kg^{-1}). X_{LF} is mainly influenced by paramagnetic minerals, as revealed by the low values of X_{ferri}. However, abnormally high values of X_{LF} are observed at *c.* 10 and 12 m, in an interval around E2 affected, among other things, by the presence of glauconitic beds.

4.d. J-meter magnetic parameters

4.d.1. Loubieng
The results of the magnetic parameters measured in Loubieng are shown in Figure 5. The IRM$_{-0.5\,T}$ is commonly lower than 0.25 mA m^2 kg^{-1} throughout the section. However, higher IRM$_{-0.5\,T}$ values are found in 'yellow' and 'red' samples. Decomposition of the IRM$_{-0.5\,T}$ into ferrimagnetic (IRM$_{-0.3\,T}$) and high-coercivity contributions (ΔIRM) shows that these samples have low ΔIRM
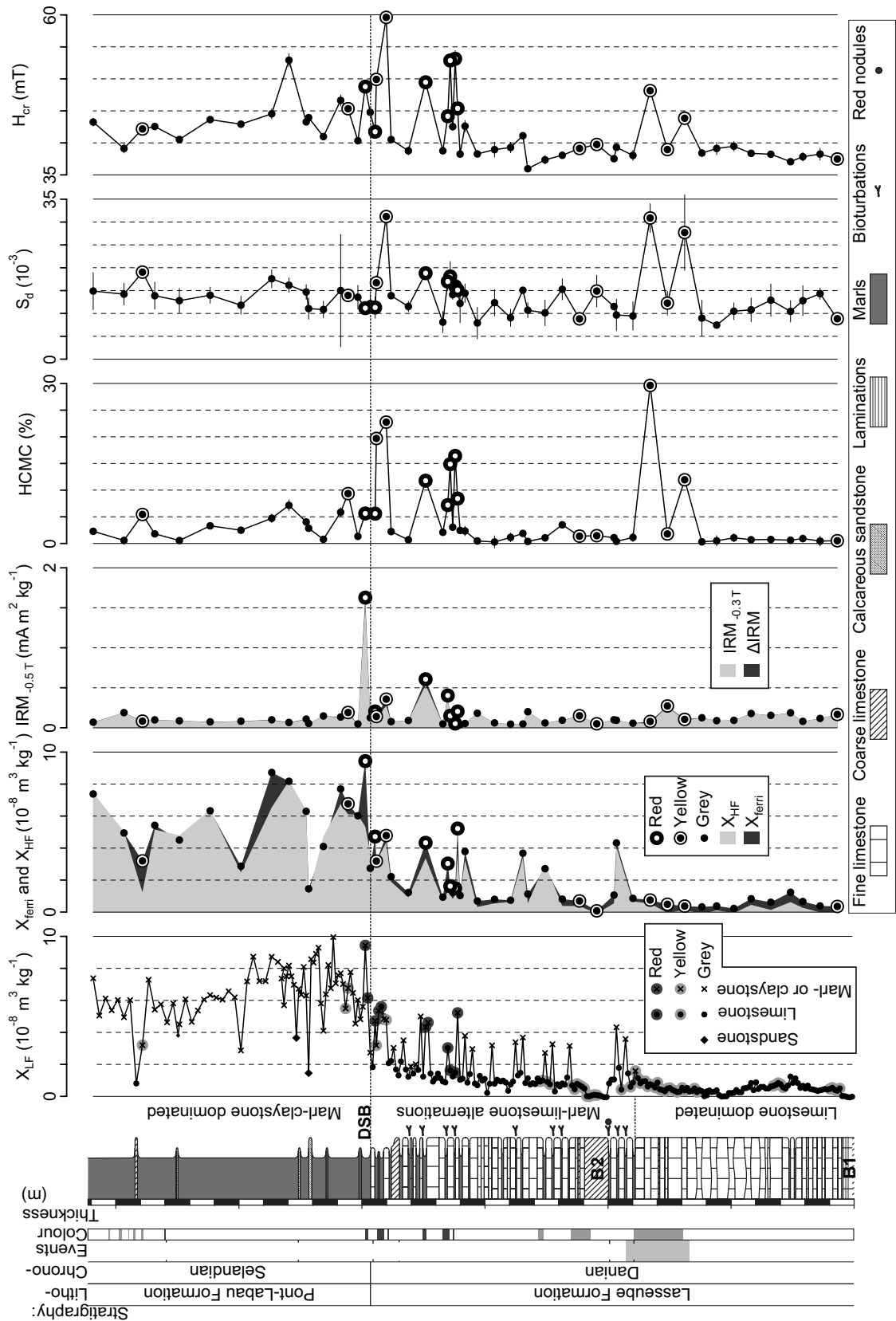
Fig. 5. Magnetic parameters for the Loubieng section. The error bar is for 2σ for each measurement. The errors for X_{LF}, X_{HF} and X_{ferri} are not provided but are typically smaller than the symbols. If the error bar is absent for all other parameters it means the error is smaller than the symbols. See Table 1 for further details on the isotopic data. R – red; Y – yellow.
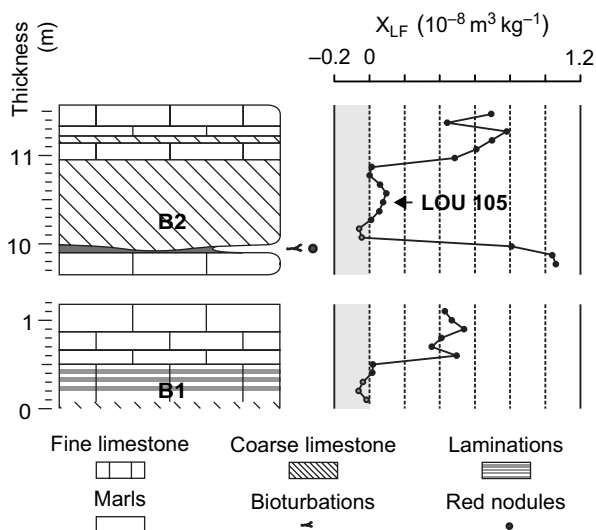
Fig. 6. Close-up view of magnetic susceptibility in beds B1 and B2 of the Loubieng section.

values. This implies that the high IRM$_{-0.5\ T}$ values (i.e. the magnetization at −0.5 T) come from a relatively important low-coercivity mineral content (e.g. magnetite) rather than only from haematite or goethite as the colour would suggest. High IRM peaks associated with 'red' samples are related to high X$_{ferri}$ values, ranging from 0.4 to 4 × 10^{-8} m^3 kg^{-1}, further confirming the importance of low-coercivity minerals. High HCMC and H$_{cr}$ values (up to 30 % for HCMC) in 'red' and 'yellow' samples nonetheless suggest the presence of high-coercivity minerals, such as haematite and goethite. High S$_d$ values (between 20 × 10^{-3} and 35 × 10^{-3}) are found only in 'yellow' samples, indicating a viscous behaviour.

Other samples at 21 and 24 m display high X$_{ferri}$ values. As only a small part of the sample used to measure X$_{LF}$ was measured in the J-meter for X$_{HF}$, these high X$_{ferri}$ values could be due to sample heterogeneity, and are thus regarded here as non-significant. High H$_{cr}$ values are observed in a sample at 23 m. No other magnetic parameter follows this behaviour in this sample, and it does not display a 'red' or 'yellow' colour. This high H$_{cr}$ value at 23 m is thus deemed non-significant, too.

4.d.2. Zumaia

The results of the magnetic parameters of Zumaia are shown in Figure 7. The high-coercivity mineral contribution (ΔIRM) accounts for more than 50 % of IRM$_{-0.5\ T}$, suggesting that the IRM$_{-0.5\ T}$ values of the 'red' samples in Zumaia are strongly influenced by high-coercivity minerals. This is confirmed by the HCMC values for these samples ranging from 25 % to nearly 80 %. IRM$_{-0.5\ T}$ and H$_{cr}$ correlate very well with HCMC (r = 0.84 and r = 0.98, respectively).

S$_d$ and HCMC follow similar trends in the Danian part of the section, while their trends diverge above the DSB. In the Danian, samples with high H$_{cr}$ and HCMC are linked with the highest S$_d$ values: up to 30 × 10^{-3}. But in the Selandian, where the highest H$_{cr}$ and HCMC values in the section are found, the S$_d$ values are systematically lower than 20 × 10^{-3}. As S$_d$ is a parameter related to the size of the ferromagnetic minerals contributing the most to magnetization, this indicates that the size populations of the high-coercivity minerals are strongly distinct between the Danian and Selandian 'red' samples.

4.d.3. Sidi Nasseur

Magnetic parameters measured in Sidi Nasseur (Fig. 8) rarely exceed the background values. The S$_d$ values display no specific trend considering the high analytical error. Isolated high values in IRM$_{-0.5\ T}$, H$_{cr}$ or HCMC can be observed. However, in this section these three parameters are inconsistent with each other. Therefore, a broad magnetic mineralogical trend can barely be deduced. The influence of high-coercivity minerals seems very faint, as shown by the IRM$_{-0.5\ T}$ curve where mainly low-coercivity minerals contribute to the signal (the ΔIRM is negligible).

### 4.d.4. Comparison of the sections in the Day Plot

The samples of all three sections saturated at or below 0.5 T display pseudo-single domain (PSD) behaviour in the Day diagram (Fig. 9). Following Dunlop (2002), this could be attributed either to PSD-sized grains or to a mixture of grains that are between SD and MD size. Thus, the size of the low-coercivity minerals cannot be precisely determined. Roberts *et al.* (2018) suggested that the Day diagram is ambiguous for domain state diagnosis, making its interpretation more difficult. More generally, these samples do not display signs of significant SP behaviour in the Day diagram. Loubieng and Zumaia samples show similar values, whereas Sidi Nasseur samples plot closer to the 'MD' field as defined by Dunlop (2002).

## 4.e. Additional magnetic analyses with the MPMS 3 instrument

4.e.1. Loubieng

The dominance of goethite or haematite in the magnetic behaviour were established with the additional magnetic analyses performed with the MPMS 3 instrument, which then determined the choice of the hue values used to discriminate 'yellow' and 'red' samples. The results are summarized in Table 2, and shown for representative samples in Figure 2. The saturation field, i.e. the field above which the M$_{rh}$ is constant, is deduced from the hysteresis loop at 7 T. The saturation field above 6 T of some samples is linked to the presence of goethite, as it is the only common natural magnetic mineral not saturated above 5 T (Dekkers, 2007). In all these goethite-bearing samples, an unblocking temperature lower than 80 °C is observed. We thus consider that a linear regression of the IRM against temperature, at temperatures over 80 °C, fits the behaviour of other magnetic minerals at lower temperatures. This in turn allows us to calculate GC (see Section 3.d.7). The GC values in the goethite-bearing samples range between 20 and 100 %. The other samples have zero GC values and saturation magnetic fields between 2 and 4 T, which are compatible with haematite (Dekkers, 2007). At low temperatures, a small fluctuation is observed in nearly all samples in the cooling curve at *c.* −25 °C. This is interpreted as the Morin transition, a haematite magnetic phase transition that occurs below −12 °C (Özdemir *et al.* 2008). The temperature of this transition can be lowered in low grain-sized haematite (to −23 °C for *c.* 0.1 μm grains, but dramatically lower for increasingly lower sizes) or with cation substitution (1 % Ti substitution suppressing the Morin transition below 10 K), and is further dependent on lattice defects, pressure and applied field (Bowles *et al.* 2010). The Morin transition is, however, not observed in sample LOU084. This could be explained either by the absence of haematite (with goethite as the only high-coercivity mineral in that sample) or by lowering of the temperature of the Morin transition (for instance owing to cation substitution or low grain size; Bowles *et al.* 2010). However, the first explanation is here
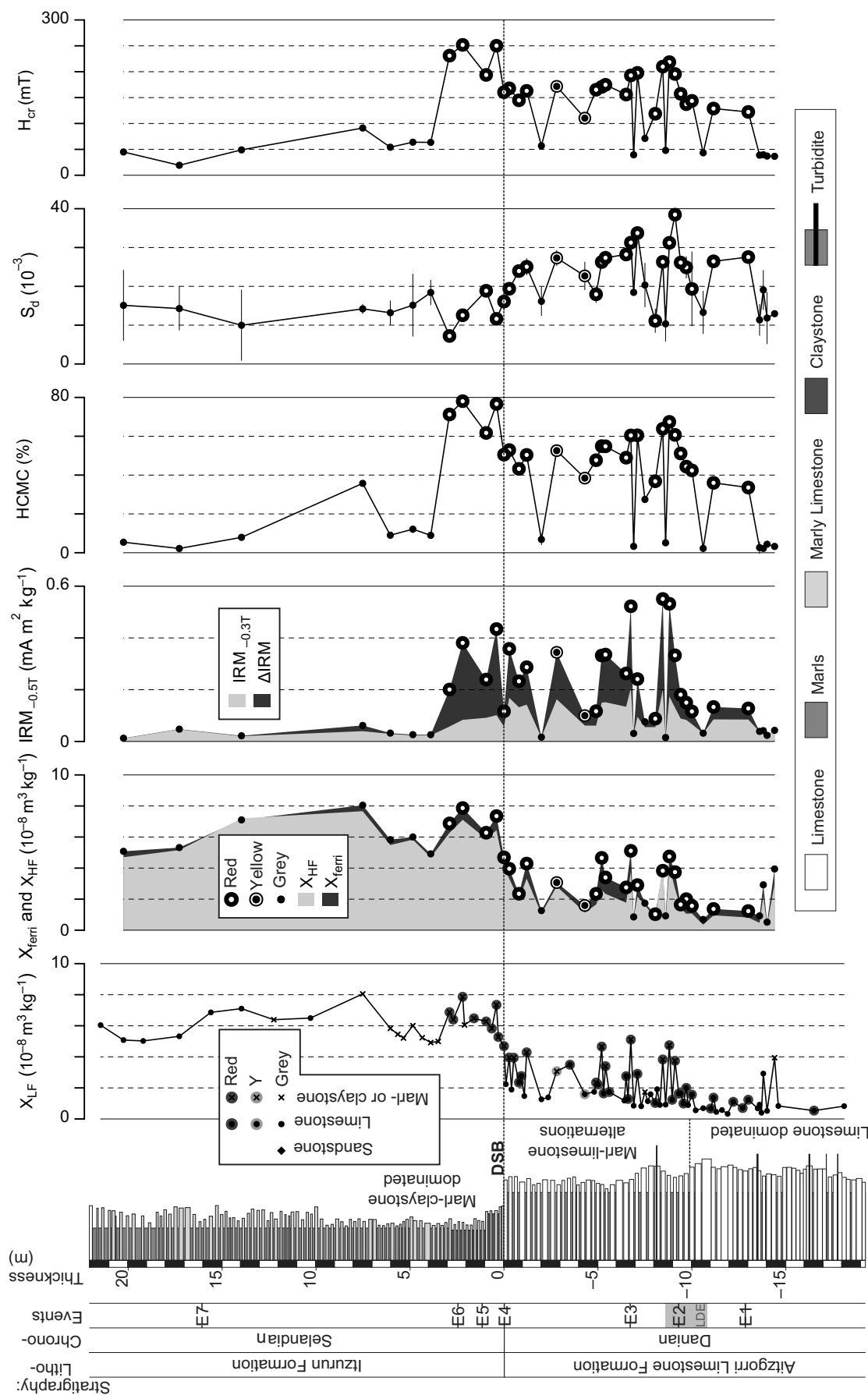
Fig. 7. Magnetic parameters for the Zumaia section. The error bar is for 2σ. The errors for X_{LF}, X_{HF} and X_{ferri} are not provided but are typically smaller than the symbols. If the error bar is absent for all other parameters it means the error is smaller than the symbols. The log was taken from Storme *et al.* (2014); see Table 1 for further details on the isotopic data.
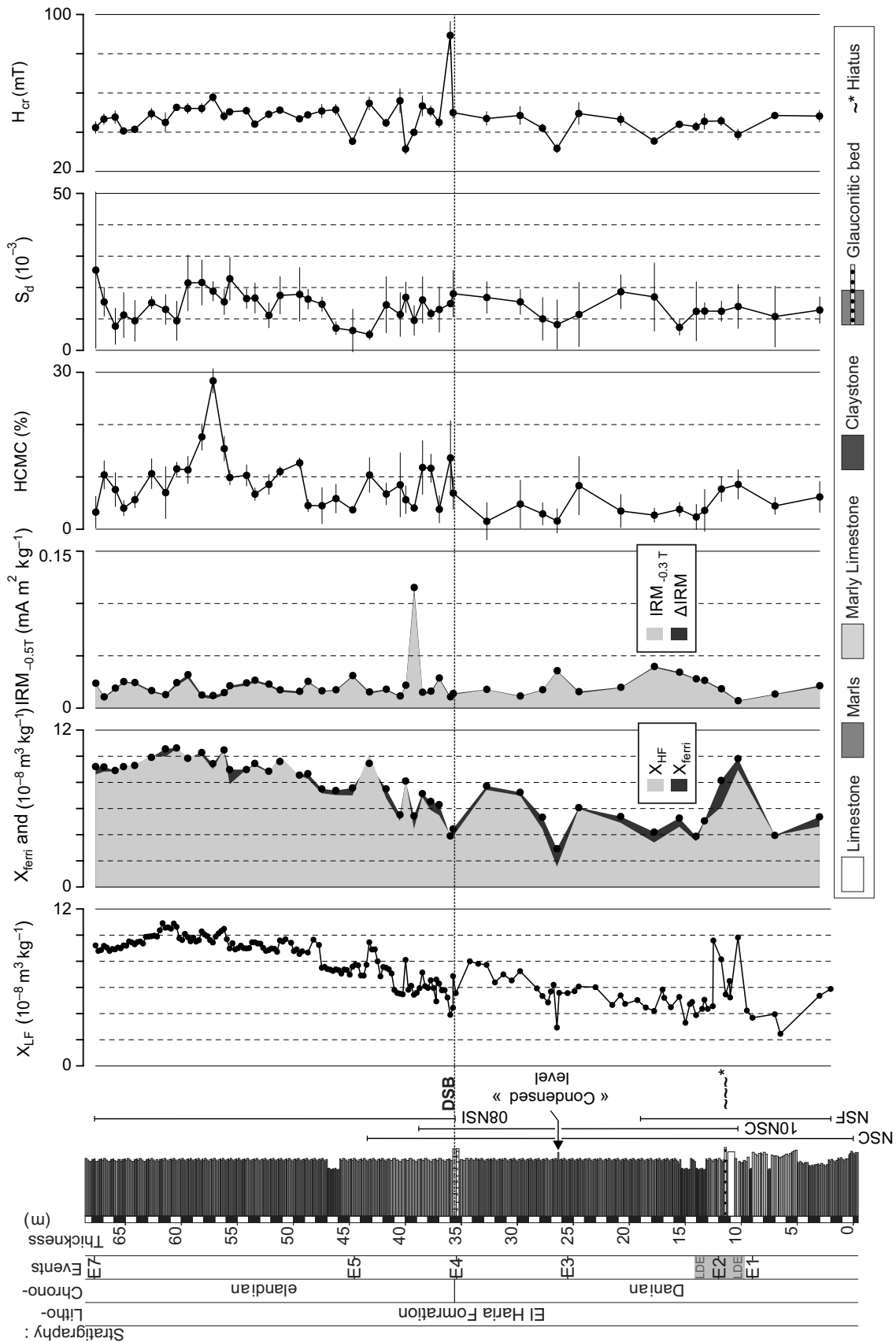
Fig. 8. Magnetic parameters for the Sidi Nasseur section. The error bar is for 2σ. The errors for X_{LF}, X_{HF} and X_{ferri} are not provided but are typically smaller than the symbols. If the error bar is absent for all other parameters it means the error is smaller than the symbols. The log comes from Storme et al. (2014); see Table 1 for further details on the isotopic data. The position of the subsections making up the composite sections (NSF, NSC, 08NSI, 10NSC) is also provided (at the right of the litholog).

Table 2. Summary of the additional MPMS 3 magnetic analyses results and comparison with colour and J-meter magnetic parameters (HCMC, H_{cr} and S_d) for the Loubieng section

Sample	Height (m)	Saturation field (T)	Goethite contribution (%)	Morin transition	Colour	HCMC (%)	H_{cr} (mT)	S_d
LOU070	6.90	Not measured	75	Strong	'yellow': 10YR 8/2	11.94	43.85	27.70
LOU084	8.30	>6	100	Absent	'yellow': 10YR 8/4	29.62	48.16	30.88
LOU162	16.12	2	0	Strong	'red': 5YR 4/4	7.96	47.04	17.51
LOU163	16.22	>6	20	Strong	'red': 10R 6/2	16.42	53.14	15.95
LOU175	17.42	4	0	Weak	'red': 5YR 5/4	12.53	51.25	20.25
LOU191	19.02	>6	41	Weak	'yellow': 10YR 6/2	22.75	59.60	31.19
LOU195	19.42	>6	48	Weak	'yellow': 10YR 6/2	19.68	49.92	16.72
LOU304	19.87	4	0	Not measured	'red': 5YR 5/4	5.62	48.79	11.64
LOU363	28.92	>6	>0	Medium	'yellow': 10YR 6/6	5.44	42.17	19.04
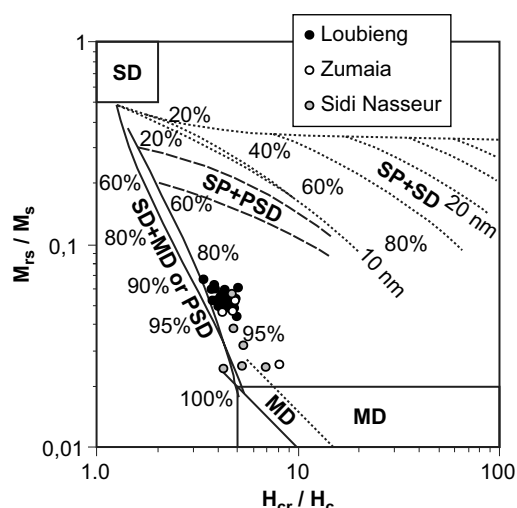
Fig. 9. Day plot for Loubieng, Zumaia and Sidi Nasseur samples with HCMC < 5 %, which excludes 'yellow' and 'red' samples, because of their high-coercivity mineral contribution making a high-field slope correction meaningless. The mixing lines are redrawn from Dunlop (2002). SD – single domain; PSD – pseudo-single domain; MD – multidomain; SP – superparamagnetic.

preferred, as the GC value is 100 %. Based on the saturation field and the GC parameter, it is possible to determine which high-coercivity mineral dominates the signal in each sample. The effect on the sample's hue is clear: the dominance of goethite (or more precisely a GC value above 40 %) coincides with a hue of 10YR, while the colour of more reddish samples coincides with the dominance of haematite (GC ≤ 20 %).

The analyses of three samples are compared in Figure 2. The displayed samples show the presence of high-coercivity minerals: haematite (LOU162), a mix of haematite and goethite (LOU195) and goethite (LOU084). Sample LOU084 displays a perfect reversibility of the remanent magnetization against temperature during cooling, which is not the case when haematite is present. It also shows an increasing slope of the IRM against the magnetic field at 0.3 T, indicating the presence of a magnetic mineral with higher coercivity than in LOU162 and LOU195.

4.e.2. Zumaia

Additional magnetic analyses were performed on four samples at Zumaia. The results are shown in Table 3. For three 'red' samples, the 'room-temperature' hysteresis loops and IRM against temperature data, respectively, reveal saturation fields of between 1 and 4 T and the presence of the Morin transition between −74 and −33 °C. The presence of haematite in these three 'red' samples is thus confirmed and linked to their colour. A fourth 'grey' sample, 08ZMS03, which has a HCMC of 35 %, does not display the Morin transition. The saturation field of this sample could not be determined with certainty because of its weak magnetization that was at the source of a low S/N ratio.

4.e.3. Sidi Nasseur

Sidi Nasseur is not studied using the MPMS 3 because of the absence of evidence for high-coercivity minerals.

4.f. Organic carbon isotopes ($\delta^{13}C_{org}$)

The $\delta^{13}C_{org}$ values dataset is provided in Tables S1–S6 in the online Supplementary Material.

4.f.1. Sidi Nasseur

The $\delta^{13}C_{org}$ trends at Sidi Nasseur are divided into four large-scale carbon isotopic excursions (CIEs): CIE-Dan1, CIE-Dan2, CIE-Sel1 and CIE-Sel2 (Fig. 3). These CIEs were first defined in Sidi Nasseur, where they are the most clearly expressed, and then correlated to Zumaia and Loubieng. In Sidi Nasseur, the onset of CIE-Dan1 is at 3 m, with $\delta^{13}C_{org}$ values at *c.* −27.4 ‰. These values decrease to −28.8 ‰ at 10 m, and then increase to reach values stabilizing at *c.* −28.0 ‰ at 23 m, defining the end of CIE-Dan1. In CIE-Dan2, starting at 23 m, the $\delta^{13}C_{org}$ values first decrease to −28.7 ‰ at 27 m and then increase to −26.7 ‰ at 36 m, above the DSB. A series of negative shifts of −1 ‰ are documented in the Danian at 10, 13, 17 and 27 m. A third negative CIE starts from the DSB and goes up to 50 m, where an inflection point changes the curvature, starting the positive CIE-Sel2. The trend made by the successive sequences of CIE-Sel1 and 2 starts with a decrease in $\delta^{13}C_{org}$ values from −26.7 ‰ at 36 m to a minimum of −28.4 ‰ at 46 m, followed by an increase to reach a maximum of −26.3 ‰

Table 3. Summary of the additional MPMS 3 magnetic analyses results and comparison with colour and J-meter magnetic parameters (HCMC, H_{cr} and S_d) for the Zumaia section

Sample	Height (m)	Saturation field (T)	Morin transition	Colour	HCMC (%)	H_{cr} (mT)	S_d
10ZMD7	−13.00	1	Medium	'red': 5YR 7/2	33.59	122.22	27.54
10ZMD37	−6.75	3	Medium	'red': 10R 4/2	60.43	192.86	31.26
11ZMX3	0.40	4	Strong	'red': 5YR 5/2	76.64	250.14	11.63
08ZMS03	7.52	Not measured	Not observed	'grey': N7	35.73	91.22	14.20

between 55 and 60 m. Values then decrease to −27.4 ‰ at the top of the series.

4.f.2. Zumaia

The $\delta^{13}C_{org}$ values in Zumaia (Fig. 3) start at −24.2 ‰ at the bottom of the section, decrease to −25.6 ‰ at −18 m, and increase again up to −23.7 ‰ at −14 m. From −14 m up to the DSB, the $\delta^{13}C_{org}$ series shows two large negative CIEs. CIE-Dan1 is found between −14 and −8 m, and is distinguished by $\delta^{13}C_{org}$ values which decrease from −23.7 ‰ to a minimum of −26.4 ‰ at −10 m and increase to −24.6 ‰ at −8 m. CIE-Dan2, found between −8 m and the DSB, is marked by $\delta^{13}C_{org}$ values that start at −24.6 ‰ at −8 m, decrease to −26.2 ‰ between −5 and −1 m, and then increase to −25.5 ‰ right below the DSB. In CIE-Dan1 and 2, smaller negative shifts are observed with an amplitude of −1 ‰ or more between −10 and −7 m. Above the DSB, we attribute CIE-Sel2 to an increase in $\delta^{13}C_{org}$ values from −25.5 ‰ to −24.6 ‰ at 3 m and a decrease down to −25.7 ‰ at 7.5 m. After 7.5 m, the $\delta^{13}C_{org}$ values increase to −24.7 ‰ at 14 m and decrease to −26.9 ‰ at the top of the section.

4.f.3. Loubieng

The isotopic geochemistry of the Loubieng section was studied in two batches of samples (Fig. 3). The $\delta^{13}C_{org}$ values of batch 1 decrease from −26.3 ‰ at the bottom of the section to −27.1 ‰ at 2.5 m. The values then tend to stabilize at *c.* −27 ‰ up to 16 m. The $\delta^{13}C_{org}$ values tend to increase from −26.8 ‰ at 16 m to −25.8 ‰ at 18.5 m. Just below the DSB, values decrease back to *c.* −26.6 ‰, which is the mean value going through the boundary. In the Selandian, CIE-DS1 is hinted at by a few samples: $\delta^{13}C_{org}$ values increase from −27.2 ‰ to −25.3 ‰, and then undergo a decrease of 0.6 ‰ at the end of the section.

The $\delta^{13}C_{org}$ values for batch 2 tend to increase from −26.1 ‰ at 3 m to −25.5 ‰ at 12 m (Fig. 3). Small-scale shifts are found at 7 m with an amplitude of −1.5 ‰, at 8.5 m with a positive shift of 2.2 ‰ and at 9 m with a negative shift of −1.1 ‰

4.f.4. General stratigraphic framework

A general chemostratigraphic framework was established from the correlation of the different CIEs, which was based on the biostratigraphic E-events (Fig. 3). Nonetheless, the position of E7 is in conflict with CIE-Sel2 in Zumaia and Sidi Nasseur. Apart from this problem, the CIEs are well correlated between the three sections.

The LDE isotopic anomaly should be coeval with bio-event E2, marking the P3a/P3b boundary (Bornemann *et al.* 2009). Based on this bio-event E2, small-scale $\delta^{13}C_{org}$ negative shifts can be attributed to the LDE (at *c.* 7 m in Loubieng, *c.* −9 m in Zumaia and *c.* 11 m in Sidi Nasseur; Fig. 3). These shifts are found in the larger $\delta^{13}C_{org}$ trend made by CIE-Dan1. In all three sections, we associate the LDE with two successive $\delta^{13}C_{org}$ negative excursions rather than only one (Fig. 3), in agreement with observations reported

in other sections (Deprez *et al.* 2017). It should be noted that similar $\delta^{13}C_{org}$ negative shifts can be found in other intervals of the studied sections.

5. Discussion

5.a. Geological meaning of the magnetic parameters

5.a.1. Magnetic susceptibility

In Loubieng and Zumaia, MS generally follows the lithological changes (Figs 5, 7) and X_{LF} usually reflects X_{HF}. This implies that the X_{LF} changes throughout the sections can be mainly explained by variations in paramagnetic mineral content, such as clays, throughout the section. Nonetheless, high X_{ferri} values in certain samples indicate the locally important influence of ferrimagnetic minerals on X_{LF}. These minerals strongly increase X_{LF}, independently from lithology. At Loubieng and Zumaia, X_{LF} can thus be used as a proxy for paramagnetic minerals and terrigenous input, provided that X_{ferri} is low and that X_{LF} follows the lithological changes. This impacts any high-resolution analysis of MS results, which should be constrained by sample-by-sample lithological observations.

At Sidi Nasseur, ferromagnetic minerals have no significant effect on the X_{LF}, as suggested by the lack of consistency between the magnetic parameters and low values in X_{ferri} and ΔIRM. Thus, paramagnetic minerals control the X_{LF} signal in Sidi Nasseur, which can be reliably used as a proxy for terrigenous input. However, high X_{LF} values during the LDE could be due to the presence of localized glauconitic beds, and may therefore not be used to follow detrital changes in this interval.

The 'red' levels in Loubieng can be found in combination with relatively high concentrations of low-coercivity minerals, as indicated by the high values in $IRM_{−0.3\ T}$ and X_{ferri} (Fig. 4). This can be interpreted as a simultaneous input of low- and high-coercivity minerals, or as the oxidation of primary low-coercivity minerals to haematite. Regardless of the interpretation, 'red' beds can indicate the presence of ferromagnetic minerals in sufficient amounts to affect the MS signal. This further highlights the need to check each sample for lithology and colour variations when interpreting X_{LF} as a proxy for paramagnetic minerals.

5.a.2. J-meter magnetic parameters

In the Loubieng and Zumaia sections, the J-meter magnetic parameters show a consistent link to colour. Coloured samples in both sections have high values of HCMC and H_{cr}, two parameters related to the presence of high-coercivity minerals. At Zumaia, coloured samples even have high ΔIRM values, indicating that a significant part of the magnetization is due to these high-coercivity minerals. This link between magnetic parameters and colour thus suggests that high-coercivity minerals are at the origins of the observed colours. The proxy for viscous decay of magnetization,

S_d, shows high values in specific coloured samples only (see Sections 5.b and 5.c). In given intervals, HCMC, H_{cr} and S_d show similar trends in similar samples (i.e. having the same colour). This indicates that these parameters are all controlled by one population of magnetic minerals at a time.

All 'red' and 'yellow' samples selected for analysis with the MPMS 3 display conclusive evidence for the presence of haematite and/or goethite in Loubieng and Zumaia. In addition, goethite dominates in 'yellow' levels (hue of 10YR) and haematite in 'red' ones (hue of 10R and 5YR). Thus, a simple comparison to a colour chart could be used to identify these two minerals and estimate their relative proportions. The magnetic parameters obtained for these samples with the J-meter also indicate the presence of these high-coercivity minerals. HCMC can be used to detect high-coercivity minerals when it is higher than the background, even with relatively low values (just above 5 %; see samples LOU304 and LOU363 in Table 2). However, it should be kept in mind that this parameter is a ratio, for which high values can arise simply from analytical variability. Therefore, high values in HCMC, e.g. 35 % for the 'grey' sample 08ZMS03 (Table 3), must be regarded with caution in very weakly magnetic samples to avoid false positives. Furthermore, seemingly significant values of H_{cr}, $IRM_{-0.5\ T}$, or X_{ferri} in certain samples lack further evidence of ferromagnetic mineral presence. In these cases the parameters cannot be interpreted meaningfully. And in some cases, the strong analytical variability of the parameters entirely prevents interpretation of any fluctuation (such as for S_d in Sidi Nasseur; Fig. 8).

5.b. Coloured levels in Loubieng

The particularly strong 'yellow' colours (10YR) overprint the bioturbation features (Fig. 4a–d), implying a post-depositional origin. In addition, the viscous behaviour of these 'yellow' levels is significantly higher than in the surrounding samples ($S_d > 20 \times 10^{-3}$). A link between post-depositional formation and viscous behaviour is therefore suggested for goethite in this section. A comparable link between chemical remagnetization (i.e. remagnetization through the formation of post-depositional minerals) and magnetic behaviour attributable to low grain size has already been noted several times in the past in carbonate rocks (e.g. Jackson & Swanson-Hysell, 2012). For instance the Morin transition could not be observed in secondary haematite from fracture and fault zones (Zwing *et al.* 2005). This could be due to low grain size, which would lower the Morin temperature and prevent its detection in the tested temperature ranges. Nonetheless, other processes could also explain this, such as cation substitution in the haematite (Bowles *et al.* 2010). Authigenic magnetite in remagnetized limestones is also known to have viscous or SP behaviour (Jackson & Swanson-Hysell, 2012).

The colour distribution, and the distribution of the haematite pigment of the 'red' levels of Loubieng, is affected by bioturbation (cf. Section 4.b.1). Primary haematite as well as very early diagenetic haematite could have been added in the recently deposited sediment and then have been mixed by burrowing benthic organisms, giving the colour distributions observed in the polished sections. However, bioturbation can change the porosity, oxygen concentration and organic matter content in the sediment. The physical difference between the bioturbated and non-bioturbated sediment could, therefore, also affect the distribution of haematite that would form after bioturbation, at least before cementation impeded the mobility of the ions needed to form the oxides. Low organic matter content in the Loubieng section (S. Wouters,

unpub. M.Sc. thesis, Université Libre de Bruxelles, 2016) is consistent with oxic conditions allowing haematite formation. Nonetheless, this does not necessarily imply an authigenic origin of this haematite. More importantly, we observe no consistency in the way bioturbation affects colour: the bioturbation features are neither systematically redder than the surrounding sediments nor systematically less red. Both cases can be observed (arrows in Fig. 4j, k). This behaviour is most easily explained by the bioturbation of sediments that already have different concentrations of red pigment. A very late diagenetic origin seems thus less probable.

5.c. Coloured levels in Zumaia

The 'red' levels of Zumaia can be divided in two groups, Danian and Selandian, based on the S_d parameter. Danian 'red' levels have S_d values mostly above 20×10^{-3}, while Selandian 'red' levels have S_d values lower than 20×10^{-3}. This threshold is identical to the one chosen in Loubieng. As both groups have samples with high HCMC, this difference is not explained by the dilution of the magnetic signal of haematite by another magnetic mineral. Conversely, the origin of haematite could be different between the Danian and the Selandian. A hypothesis could be that the Danian haematite is of post-depositional origin. Dinarès-Turell *et al.* (2010) formulated an early diagenetic origin for the fine and pigmentary haematite in these levels. On the other hand, the Selandian haematite could be at least partly primary, and made of coarser grains than in the Danian. This would imply a relationship between the grain size, viscous behaviour and diagenetic origin of a magnetic mineral, in this case haematite. This hypothesis could explain why 'red' levels in Loubieng are observed only near the DSB while in Zumaia they are found much earlier. Primary haematite would have been deposited around the DSB in both sections, and haematite in the Danian beds of Zumaia would have formed after sedimentation by diagenetic processes. That would thus imply a primary origin for the haematite at Loubieng. However, this cannot be confirmed by the S_d parameter in Loubieng, as the HCMC is low, which implies that the S_d parameter is related to low-coercivity minerals.

5.d. Gravitational deposits in Loubieng

At Loubieng, event deposits display abnormally low X_{LF} values compared to the other beds of the series (Fig. 5). In the Danian, these are the metric B1 and B2 beds and two thinner beds at 5.2 and 6 m in the zone where beds are lenticular. These limestone beds have a different microfacies than the surrounding limestone beds. Their microfacies are bioclastic packstones containing micritic clasts and bioclasts having clear neritic origins (like red algae), while the other limestone beds consist of planktonic *Globigerina* and *Globotruncana* mudstones to wackestones, indicating a more pelagic setting (S. Wouters, unpub. M.Sc. thesis, Université Libre de Bruxelles, 2016). A close-up view of the MS values in B1 and B2 (Fig. 6) shows negative X_{LF} values at the bottom of both beds. This indicates a magnetic behaviour dominated by diamagnetic minerals and thus a very low concentration of paramagnetic (usually clays) and ferromagnetic minerals. The sample LOU105, which was taken in B2 and measured using the J-meter, has an X_{HF} of -8×10^{-10} m^3 kg^{-1} and a X_{LF} of 8×10^{-10} m^3 kg^{-1}. These data indicate the presence of mainly diamagnetic (carbonates) and ferrimagnetic minerals, and the absence of a significant clay contribution to the signal. The HCMC is 1.5 %, confirming that low-coercivity minerals are the main ferromagnetic minerals in that sample. In B2, the highest MS values are found in the centre

of the bed. Altogether this would imply that ferrimagnetic minerals are concentrated there. This argument, combined with the presence of an erosive surface at the bottom of the bed and a microfacies typical of a shallow water carbonate platform environment, indicates that these beds are the record of gravitational deposits which had enough velocity to erode underlying sediments and have a size-dependent redistribution of the minerals within the bed. This latter effect would be responsible for the distribution of low-coercivity minerals in the centre of the bed. The two thin lenticular beds found at 5.2 and 6 m were previously identified as slumps (Peybernès *et al.* 2000; Rocher *et al.* 2000), but facies and low X_{LF} values also suggest that these beds are energetic gravitational deposits as well, bringing proximal material from the shallow water platform into the deep basinal setting of Loubieng.

In the Selandian, a few sandstone and red algae limestone beds (S. Wouters, unpub. M.Sc. thesis, Université Libre de Bruxelles, 2016) display low MS values. Again, these are attributed to gravitational deposits as they are made of material allochthonous to the pelagic setting of Loubieng.

5.e. Depositional changes during the Danian–Selandian transition

Dinarès-Turell *et al.* (2010) ascribed the marl–limestone couplets in Loubieng to precession cycles. Such lithological alternations in other sections have already been attributed to cyclic climate changes where marl beds were deposited under tropical humid conditions and limestone beds under semi-arid conditions (Mutterlose & Ruffell, 1999; Moiroud *et al.* 2012). This implies that the X_{LF} signal, which mainly follows the expression of these alternations, would be linked to climate. At a larger scale, and still based on MS, the section is divided into three intervals. The interval boundaries are at the E2 and E4 bio-events (Fig. 3), and are linked to the LDE and the DSB, respectively. They both mark sudden increases in detrital input. A more gradual increase in detrital input can be observed in Loubieng before E2 and E4 by the increase in X_{LF} in the limestones (at *c.* 8 m and *c.* 19 m; Fig. 3).

The marl–limestone alternations at Zumaia are also attributed to precession cycles (Dinarès-Turell *et al.* 2010). The lithological contrast is expressed in the X_{LF} signal, suggesting a similar link between climate and X_{LF} as in Loubieng. Also as in Loubieng, the Zumaia section can be divided into three intervals using the bio-events E2 and E4 as boundaries (Fig. 7). A smooth increase in the X_{LF} values in the limestone beds before the DSB is observed, followed by a stronger increase right at the DSB.

Sidi Nasseur shows monotonous X_{LF} characteristics. Hence, clear precession-scale alternations such as those found in Loubieng and Zumaia cannot be clearly observed with our sampling rate. This implies that the X_{LF} signal acquired for Sidi Nasseur can only be used to study long-term effects. These long-terms effects could be related to the E2 and E4 events, but as their expression is different than in Loubieng and Zumaia, and are less clearly expressed, this interpretation would be subject to caution.

The three sections all display a long-term increase in terrigenous input from the upper Danian part of the series to the DSB. At Loubieng and Zumaia, the same abrupt X_{LF} increase is observed at the DSB, while in Sidi Nasseur this increase is gentler, indicating a discrepancy between the Atlantic and Tethyan sections. Still, the long-term increase in terrigenous input throughout the studied interval, observed by the X_{LF} fluctuations and found consistently in all three sections, allows X_{LF} to be used for large-scale correlations.

A discrepancy between the Atlantic and Tethyan sections is put forward by the fact that the CIE-Sel1 $\delta^{13}C_{org}$ trend found in Sidi Nasseur is not clearly observed in Loubieng and Zumaia. This CIE is hinted at between E4 and E5 in Zumaia, but would be concentrated in 1 m of sediments. This points towards low sedimentation rates after the DSB in Loubieng and Zumaia, relative to the other parts of the sections.

In CIE-Sel2, the X_{LF} values follow a similar trend in all three sections, with an increasing and then decreasing trend. These particular trends are concentrated in 3 m in Zumaia, while covering more than 7 m in Loubieng and more than 20 m in Sidi Nasseur. This indicates that Zumaia has a more condensed nature than the other sections in this interval. This is confirmed by the results of Storme *et al.* (2014), which showed that the CIE-Sel2 event itself constitutes 6 m in Zumaia, while it encompasses more than 11 m in Loubieng and more than 23 m in Sidi Nasseur. The low sedimentation rate in the basal Selandian observed in the Zumaia section is confirmed by biostratigraphy, with the E-events E4, E5 and E6 following each other in a small interval at the bottom of the Selandian at Zumaia.

The hyperthermal event of *c.* 30 kyr at the very beginning of the Selandian proposed by Storme *et al.* (2014) occurs during a haematite influx event observed in Loubieng and Zumaia. This influx could be due to dry climatic conditions in the gulf of the Biscay area, leading to the formation of haematite in soils. However, the red levels in Zumaia and Loubieng do not correlate clearly, as the primary haematite is found only in the Selandian of Zumaia, whereas it can also be found below the DSB in Loubieng. Furthermore, primary haematite can also originate from the mechanical erosion of haematite-bearing deposits that would have formed earlier. Therefore, a tectonic effect exposing such deposits could equally explain this primary haematite.

Most strikingly, in Loubieng, the start of the gradual increase in X_{LF} before E2 is synchronous with the start of the LDE as we define it based on carbon isotopes, and the start of the gradual increase in X_{LF} before the DSB is synchronous with the first occurrence of the primary red layers. This implies that the increase in lithogenic input is directly related to the suggested climatic events.

6. Conclusions

Magnetic susceptibility data reveals similar patterns or trends in the three sections: patterns linked to a precession-related climatic effect that creates marl–limestone alternations in Loubieng and Zumaia. X_{LF} is interpreted as a proxy for terrigenous input when controlled by paramagnetic minerals, as is the case for most of the samples studied here. However, a minority of samples still show significant ferromagnetic contributions. This underlines the need for techniques discriminating paramagnetic and ferromagnetic minerals to confirm that paramagnetic minerals are controlling X_{LF}, especially when high-resolution fluctuations are studied (e.g. in cyclostratigraphy). The J-meter proves to be a useful tool in that regard. In the case of Loubieng and Zumaia, the J-meter also allowed the detection and characterization of high-coercivity minerals, even if the maximum magnetic field of 0.5 T is not enough to saturate them. However, when using the J-meter it is important to estimate the significance of the magnetic parameters. Minimizing the risk of over-interpretation of X_{LF} variations can further be accomplished using simple colour and lithological observations. Furthermore, the comparison of coeval sections allows us to confirm the global significance of the local observations.

Haematite and goethite are identified and characterized by their colour and magnetic properties. Their identification can help the interpretation of X_{LF} data, as such minerals can affect that measurement or indicate the presence of other low-coercivity minerals. In Loubieng, the overprinting of bioturbation features by goethite-bearing 'yellow' levels suggests a post-depositional origin of that goethite. Also in Loubieng, the mixing of 'red' shades by bioturbation indicates an earlier origin for the haematite. In Zumaia, the 'red' levels could be divided based on the S_d parameter. This seems to indicate different origins: primary for low S_d Danian 'red' beds, and diagenetic for high S_d Selandian 'red' beds. As the diagenetic goethite in Loubieng also displays low S_d values and could be of primary origin, this could mean that the viscous magnetization parameter S_d could be useful for identifying post-depositional minerals. But additional studies are needed to validate or disprove this hypothesis.

Indeed, it should be kept in mind that rock-magnetic analyses are a double-edged sword. Their sensitivity allows profound insight into the magnetic mineralogy of rocks. However, as that insight is difficult to match to other methods commonly used, linking the results of magnetic analyses back to geological processes is difficult. This makes these techniques very prone to over-interpretation. Therefore, for magnetic techniques, it is only by challenging hypotheses in a variety of settings that we will verify them.

Comparison between the sections is based on newly identified $\delta^{13}C_{org}$ excursions defined first in Sidi Nasseur (CIE-Dan1 and 2, CIE-Sel1 and 2). It correlates well with X_{LF} trends and biostratigraphy and shows the condensed nature of the interval after the DSB in the Atlantic sections. The Zumaia section seems to have the lowest sedimentation rate at the base of the Selandian, which could be problematic as it is the GSSP of that stage. Sidi Nasseur on the other hand shows a much more expanded record.

The origin of the 'red' beds of Loubieng and of the Selandian in Zumaia are interpreted as being of primary origin, implying a continental origin due to either dry climatic conditions or erosion of haematite-bearing deposits. In the case of a climatic origin, this would indicate drier climatic conditions. This locally corroborates the hyperthermal event hypothesized by Storme *et al.* (2014) for the basal Selandian, but needs to be confirmed.

In Loubieng, the LDE and the influx of haematite are both synchronous with a gradual increase in lithogenic influx. This further confirms a strong link between lithogenic influxes and climatic events. As the increase in lithogenic influxes remains after the short-lived climatic events that happened at the DSB and LDE, it can be inferred that these climate changes are either linked to the culmination of longer-lived processes, or have effects lasting long after their conclusion.

Author ORCIDs. (iD) Sébastien Wouters 0000-0003-2526-0880

References

Abrajevitch A, der Voo RV and Rea DK (2009) Variations in relative abundances of goethite and hematite in Bengal Fan sediments: climatic vs. diagenetic signals. *Marine Geology* **267**, 191–206.

Arenillas I, Molina E, Ortiz S and Schmitz B (2008) Foraminiferal and δ^{13}C isotopic event-stratigraphy across the Danian–Selandian transition at Zumaya (northern Spain): chronostratigraphic implications. *Terra Nova* **20**, 38–44.

Bernaola G, Martín-Rubio M and Baceta JI (2009) New high resolution calcareous nannofossil analysis across the Danian/Selandian transition at the Zumaia Section: comparison with South Tethys and Danish sections. *Geologica Acta* **7**, 79–92.

Bornemann A, Schulte P, Sprong J, Steurbaut E, Youssef M and Speijer R (2009) Latest Danian carbon isotope anomaly and associated environmental change in the southern Tethys (Nile Basin, Egypt). *Journal of the Geological Society, London* **166**, 1135–42.

Bowles J, Jackson M and Banerjee SK (2010) Interpretation of low-temperature data part II: the hematite Morin transition. *IRM Quarterly* **20**, 8–10.

Da Silva AC, De Vleeschouwer D, Boulvain F, Claeys P, Fagel N, Humblet M, Mabille C, Michel J, Sardar Abadi M, Pas D and Dekkers MJ (2013) Magnetic susceptibility as a high-resolution correlation tool and as a climatic proxy in Paleozoic rocks – merits and pitfalls: examples from the Devonian in Belgium. *Marine and Petroleum Geology* **46**, 173–89.

Dekkers MJ (1989) Magnetic properties of natural goethite—II. TRM behaviour during thermal and alternating field demagnetization and low-temperature treatment. *Geophysical Journal International* **97**, 341–55.

Dekkers MJ (2007) Magnetic proxy parameters. In *Encyclopedia of Geomagnetism and Paleomagnetism* (eds D Gubbins and E Herrero-Bervera), pp. 525–34. Dordrecht: Springer.

Deprez A, Jehle S, Bornemann A and Speijer RP (2017) Pronounced biotic and environmental change across the latest Danian warming event (LDE) at Shatsky Rise, Pacific Ocean (ODP Site 1210). *Marine Micropaleontology* **137**, 31–45.

De Vleeschouwer D, Boulvain F, Da Silva A-C, Pas D, Labaye C and Claeys P (2015) The astronomical calibration of the Givetian (Middle Devonian) timescale (Dinant Synclinorium, Belgium). In *Magnetic Susceptibility Application: A Window onto Ancient Environments and Climatic Variations* (eds AC Da Silva, MT Whalen, J Hladil, L Chadimova, D Chen, S Spassov, F Boulvain and X Devleeschouwer), pp. 245–56. Geological Society of London, Special Publication no. 414.

Devleeschouwer X, Petitclerc E, Spassov S and Preat A (2010) The Givetian–Frasnian boundary at Nismes parastratotype (Belgium): the magnetic susceptibility signal controlled by ferromagnetic minerals. *Geologica Belgica* **13/4**, 351–66.

Devleeschouwer X, Riquier L, Bábek O, De Vleeshouwer D, Petitclerc E, Sterckx S and Spassov S (2015) Magnetization carriers of grey to red deep-water limestones in the GSSP of the Givetian–Frasnian boundary (Puech de La Suque, France): signals influenced by moderate diagenetic overprinting. In *Magnetic Susceptibility Application: A Window onto Ancient Environments and Climatic Variations* (eds AC Da Silva, MT Whalen, J Hladil, L Chadimova, D Chen, S Spassov, F Boulvain and X Devleeschouwer), pp. 157–80. Geological Society of London, Special Publication no. 414.

Dinarès-Turell J, Stoykova K, Baceta JI, Ivanov M and Pujalte V (2010) High-resolution intra- and interbasinal correlation of the Danian–Selandian transition (Early Paleocene): the Bjala section (Bulgaria) and the Selandian GSSP at Zumaia (Spain). *Palaeogeography, Palaeoclimatology, Palaeoecology* **297**, 511–33.

Dunlop DJ (1973) Theory of the magnetic viscosity of lunar and terrestrial rocks. *Review of Geophysics* **11**, 855–901.

Dunlop DJ (2002) Theory and application of the Day plot (Mrs/Ms versus Hcr/Hc) 1. Theoretical curves and tests using titanomagnetite data. *Journal of Geophysical Research* **107**, EPM4-1–EPM4-22, doi: 10.1029/2001JB000486

Ellwood BB, Crick RE and Hassani AE (1999) The Magneto-Susceptibility Event and Cyclostratigraphy (MSEC) method used in geological correlation

of Devonian rocks from Anti-Atlas Morocco. *American Association of Petroleum Geologists Bulletin* **83**, 1119–34.

Evans ME and Heller F (2003) *Environmental Magnetism: Principles and Applications of Enviromagnetics*. Amsterdam: Academic Press.

Fabian K and von Dobeneck T (1997) Isothermal magnetization of samples with stable Preisach function: a survey of hysteresis, remanence, and rock magnetic parameters. *Journal of Geophysical Research* **102**, 17659–77.

Gheerbrant E and Rage J-C (2006) Paleobiogeography of Africa: how distinct from Gondwana and Laurasia? *Palaeogeography, Palaeoclimatology, Palaeoecology* **241**, 224–46.

Goddard EN, Trask PD, De Ford RK, Rove ON, Singewald JT, Overbeck J and Overbeck RM (1948) *Rock-Color Chart*. Washington: National Research Council.

Guasti E, Speijer RP, Brinkhuis H, Smit J and Steurbaut E (2006) Paleoenvironmental change at the Danian–Selandian transition in Tunisia: foraminifera, organic-walled dinoflagellate cyst and calcareous nannofossil records. *Marine Micropaleontology* **59**, 210–29.

Henry J, Zolnaï G, Le Pochat G and Mondeilh C (1989) *Notice Explicative de la Feuille à 1/50000 Orthez*. Orléans: Bureau de Recherches Géologiques et Minières, 55 pp.

Jackson M and Swanson-Hysell NL (2012) Rock magnetism of remagnetized carbonate rocks: another look. In *Remagnetization and Chemical Alteration of Sedimentary Rocks* (eds RD Elmore, AR Muxworthy, MM Aldana and M Mena), pp. 229–51. Geological Society of London, Special Publication no. 371.

Kodama KP, Anastasio DJ, Newton ML, Pares JM and Hinnov LA (2010) High-resolution rock magnetic cyclostratigraphy in an Eocene flysch, Spanish Pyrenees. *Geochemistry, Geophysics, Geosystems* **11**, Q0AA07, doi: 10.1029/2010GC003069.

Kodama KP and Hinnov LA (2014) *Rock Magnetic Cyclostratigraphy*. Hoboken, NJ: John Wiley & Sons.

Liu Q, Torrent J, Maher BA, Yu Y, Deng C, Zhu R and Zhao X (2005) Quantifying grain size distribution of pedogenic magnetic particles in Chinese loess and its significance for pedogenesis. *Journal of Geophysical Research* **110**, B11102, doi: 10.1029/2005JB003726

Martinez M, Kotov S, De Vleeschouwer D, Pas D and Pälike H (2016) Testing the impact of stratigraphic uncertainty on spectral analyses of sedimentary series. *Climate of the Past Discussions* **12**, 1765–83.

Mayer H and Appel E (1999) Milankovitch cyclicity and rock-magnetic signatures of palaeoclimatic change in the Early Cretaceous Biancone Formation of the Southern Alps, Italy. *Cretaceous Research* **20**, 189–214.

Moiroud M, Martinez M, Deconinck J-F., Monna F, Pellenard P, Riquier L and Company M (2012) High-resolution clay mineralogy as a proxy for orbital tuning: example of the Hauterivian–Barremian transition in the Betic Cordillera (SE Spain). *Sedimentary Geology* **282**, 336–46.

Moskowitz BM, Frankel RB and Bazylinski DA (1993) Rock magnetic criteria for the detection of biogenic magnetite. *Earth and Planetary Science Letters* **120**, 283–300.

Mutterlose J and Ruffell A (1999) Milankovitch-scale palaeoclimate changes in pale–dark bedding rhythms from the Early Cretaceous (Hauterivian and Barremian) of eastern England and northern Germany. *Palaeogeography, Palaeoclimatology, Palaeoecology* **154**, 133–60.

Néel L (1949) Théorie du traînage magnétique des ferromagnétiques en grains fins avec applications aux terres cuites. *Annales Geophysicae* **5**, 99–136.

Özdemir Ö and Dunlop DJ (1996) Thermoremanence and Néel temperature of goethite. *Geophysical Research Letters* **23**, 921–4.

Özdemir Ö, Dunlop DJ and Berquó TS (2008) Morin transition in hematite: size dependence and thermal hysteresis. *Geochemistry, Geophysics, Geosystems* **9**, Q10Z01, doi: 10.1029/2008GC002110.

Peybernès B, Fondecave-Wallez M-J, Hottinger L, Eichène P and Segonzac G (2000) Limite Crétacé–Tertiaire et biozonation micropaléontologique du Danien–Sélandien dans le Béarn occidental et la Haute-Soule (Pyrénées-Atlantiques). *Geobios* **33**, 35–48.

Roberts AP, Tauxe L, Heslop D, Zhao X and Jiang Z (2018) A critical appraisal of the "Day" diagram. *Journal of Geophysical Research: Solid Earth* **123**, 2618–44.

Rocher M, Lacombe O, Angelier J, Deffontaines B and Verdier F (2000) Cenozoic folding and faulting in the south Aquitaine Basin (France): insights from combined structural and paleostress analyses. *Journal of Structural Geology* **22**, 627–45.

Schmitz B, Pujalte V, Molina E, Monechi S, Orue-Etxebarria X, Speijer RP, Alegret L, Apellaniz E, Arenillas I, Aubry M-P, Baceta J-I, Berggren WA, Bernaola G, Caballero F, Clemmensen A, Dinares-Turell J, Dupuis C, Heilmann-Clausen C, Hilario Orus A, Knox R, Martin-Rubio M, Ortiz S, Payros A, Petrizzo MR, von Salis K, Sprong J, Steurbaut E and Thomsen E (2011) The Global Stratotype sections and points for the bases of the Selandian (Middle Paleocene) and Thanetian (Upper Paleocene) stages at Zumaia, Spain. *Episodes* **34**, 220–43.

Steurbaut E and Sztrákos K (2008) Danian/Selandian boundary criteria and North Sea Basin–Tethys correlations based on calcareous nannofossil and foraminiferal trends in SW France. *Marine Micropaleontology* **67**, 1–29.

Storme J-Y, Steurbaut E, Devleeschouwer X, Dupuis C, Iacumin P, Rochez G and Yans J (2014) Integrated bio-chemostratigraphical correlations and climatic evolution across the Danian–Selandian boundary at low latitudes. *Palaeogeography, Palaeoclimatology, Palaeoecology* **414**, 212–24.

Van Itterbeeck J, Sprong J, Dupuis C, Speijer RP and Steurbaut E (2007) Danian/Selandian boundary stratigraphy, paleoenvironment and Ostracoda from Sidi Nasseur, Tunisia. *Marine Micropaleontology* **62**, 211–34.

Varol O (1989) Palaeocene calcareous nannofossil biostratigraphy. In *Nannofossils and their Applications: Proceedings of the International Nannofossil Association Conference, London* (eds JA Crux and SE van Heck), pp. 267–310. British Micropalaeontological Society Series. Chichester: Ellis Horwood for the British Micropalaeontological Society.

Wang X, Løvlie R, Zhao X, Yang Z, Jiang F and Wang S (2010) Quantifying ultrafine pedogenic magnetic particles in Chinese loess by monitoring viscous decay of superparamagnetism. *Geochemistry, Geophysics, Geosystems* **11**, Q10008, doi: 10.1029/2010GC003194.

Westerhold T, Röhl U, Donner B, McCarren HC and Zachos JC (2011) A complete high-resolution Paleocene benthic stable isotope record for the Central Pacific (ODP Site 1209). *Paleoceanography* **26**, PA2216, doi: 10.1029/2010PA002092.

Zwing A, Matzka J, Bachtadse V and Soffel HC (2005) Rock magnetic properties of remagnetized Palaeozoic clastic and carbonate rocks from the NE Rhenish massif, Germany. *Geophysical Journal International* **160**, 477–86.